High-Order Artificial Dissipation Operators Possessing the Summation-By-Parts Property

David A. Craig Penner* and David W. Zingg†
University of Toronto Institute for Aerospace Studies, Toronto, Ontario, M3H 5T6

The summation-by-parts (SBP) property can be used to construct high-order provably stable numerical methods. A general framework is explored for deriving provably stable and conservative artificial dissipation operators for use with high-order traditional and element-type SBP operators on general nodal distributions, thus enabling the time stable and accurate solution of practical nonlinear problems, including those problems that contain variable coefficients, for example, aerodynamics problems involving the compressible Euler and Navier-Stokes equations. The basic premise is presented for scalar conservation laws and then extended to entropy stability for systems. Artificial dissipation operators for use with traditional SBP operators are constructed having 1^{st}, 3^{rd}, 5^{th}, and 7^{th} order accuracy on the interior achieved with minimum-width stencils that have ample flexibility in the derivation of novel accuracy-preserving boundary closures. Element-type dissipation operators are constructed on the Legendre-Gauss and Legendre-Gauss-Lobatto nodal distributions. The stability and accuracy properties of a suite of the constructed artificial dissipation operators are characterized in the numerical solution of the quasi-one-dimensional Euler equations applied to a converging-diverging nozzle.

I. Introduction

The study of high-order numerical methods for the solution of partial differential equations is an active area of research due to their potential to drastically reduce the computational expense of solving large-scale scientific problems on massively parallel and heterogenous architectures. This is because high-order schemes can be demonstrably more efficent than low-order methods below a certain error tolerance [1–5]. To this end, the influential summation-by-parts (SBP) framework, initially introduced by Kreiss and Scherer [6] and later extended and refined by Strand [7], has been instrumental in enabling the construction of stable numerical methods of arbitrary order that have subsequently been used to solve an extensive class of practical and research-oriented problems across several broad disciplines including aerodynamics [8–10], fundamental physics [11], and quantum cosmology [12]. A particularly powerful methodology that combines SBP operators with simultaneous approximation terms (SATs) [13–16] to weakly enforce boundary conditions and inter-element coupling in a stable manner, hereafter referred to as the SBP-SAT approach, can form a rigorous framework under which discrete conservation and energy stability can be proven for linear problems [17–19]. In addition to providing a means for constructing stable and accurate boundary closures, the use of SATs eliminates the need for halo nodes when solving systems of equations on multi-block structured grids, which naturally fosters an efficient numerical algorithm due to reduced communication overhead when coupled with a parallel computational strategy, independent of the order of the overall discretization [10]. Furthermore, because SATs only require C^0 continuity across block interfaces, mesh continuity requirements can be judiciously relaxed at certain locations throughout the grid, which can potentially allow the consideration of more complex geometries compared to what might be possible without the use of SATs.

The stability and conservation proofs that form the foundation for the SBP-SAT approach are in large part possible because SBP operators are discretely mimetic of integration-by-parts. The majority of problems currently solved using the SBP-SAT approach employ traditional SBP operators, in which a repeated interior point operator is utilized to approximate a given derivative on a uniform nodal distribution that includes both boundary nodes. However, recently, Del Rey Fernández *et al.* extended the SBP property to encompass a larger class of operators for first and second

*Ph.D. Student, Institute for Aerospace Studies, 4925 Dufferin Street, and AIAA Student Member (david.craigpenner@mail.utoronto.ca).

†University of Toronto Distinguished Professor of Computational Aerodynamics and Sustainable Aviation, Director, Centre for Research in Sustainable Aviation, Director, Centre for Computational Science and Engineering, Institute for Aerospace Studies, 4925 Dufferin Street, and AIAA Associate Fellow (dwz@oddjob.utias.utoronto.ca).

derivatives, including the following types of operators: operators that do not have a repeated interior point operator, operators that have nonuniform nodal distributions, and operators that do not include one or both boundary nodes [20, 21]. These generalized summation-by-parts (GSBP) operators can potentially lead to flexible and efficient schemes that are arbitrarily high-order, discretely conservative, and provably stable, which motivates their further investigation and development. Truly multidimensional GSBP operators have also been derived on simplices [16, 22, 23]; however, in the present work we only consider one-dimensional operators that may be extended to multiple dimensions through the use of the tensor-product formalism.

In addition to linear problems, high-order SBP-SAT schemes can also be used to discretize nonlinear conservation laws. The wide-scale adoption of high-order methods for the solution of nonlinear problems is presently hindered in part due to stability concerns. As a result, entropy conservative and entropy stable schemes have been proposed, which seek to alleviate the stability issues associated with the practical implementation of high-order methods [23–25]. However, even for schemes that can be shown to be entropy conservative, the introduction of additional dissipation is typically necessary to ensure that the overall solution is numerically stable [23]. We are ultimately interested in the numerical solution of the compressible Euler and Navier-Stokes equations and therefore we require some additional form of artificial dissipation, which is normally provided either by incorporating upwind-type operators that inherently introduce dissipation [26], or more commonly, through the use of an artificial dissipation model [27, 28].

Artificial dissipation models for use with traditional SBP operators were initially constructed by Mattsson *et al.* [27] for both diagonal and dense norm operators. In their work, they constructed artificial dissipation operators to preserve the accuracy and stability properties of the underlying numerical scheme, while reducing unphysical oscillations in the numerical solution in a computationally efficient manner [27]. In a subsequent paper, Diener *et al.* constructed dissipation operators based on the work of [27] and evaluated their performance in the context of a scalar wave equation [28]. For nonlinear conservation laws in a practical setting, the SBP-SAT approach has been successfully applied to both the Euler and Navier-Stokes equations discretized using traditional SBP operators [8, 10], with stabilization being achieved through the use of a modified version of the classical scalar [29] and matrix [30] dissipation models. In addition, Svärd and Mishra extended [27] to handle shock capturing [31]. Alternatively, Mattsson introduced a novel definition of first derivative SBP operators that involves dual-pair upwind SBP operators having biased interior stencils to introduce numerical dissipation without the use of an artificial dissipation model; the use of these operators was subsequently shown to outperform the implementation of traditional SBP operators coupled with artificial dissipation models for certain problems [26]. More recently, Ranocha *et al.* investigated the construction of artificial dissipation operators using nodal and modal Legendre-type bases by interpreting a flux reconstruction framework using the SBP-SAT approach, characterizing the constructed operators using the energy method, and relating the final results to modal filtering [32].

The current objective is to extend the state-of-the-art of SBP-SAT compatible artificial dissipation operators by exploring a provably conservative and stable framework for their construction in the context of the SBP property as defined by Del Rey Fernández *et al.* [20], for both traditional and element-type operators. The provable stability of interest is provable time stability via the energy method that can be extended to nonlinear systems of conservation laws using entropy. This particular notion of stability is used as it is in accordance with the overall SBP-SAT approach. Note that the energy method provides a sufficient condition for time stability but not a necessary one. Furthermore, we seek to clarify the application of the constructed dissipation models to nonlinear systems of conservation laws, for example, discretizations of the Euler equations that involve the flux Jacobian matrix. Finally, we investigate an alternative framework for the construction of traditional SBP dissipation operators having minimum-width interior stencils and present a novel method for deriving stable boundary closures that preserve the accuracy of the underlying numerical scheme.

We consider systems that have been transformed using curvilinear coordinates and, as a result, we restrict ourselves to SBP-SAT discretizations constructed using diagonal norms. This restriction is necessary because in curvilinear coordinates on conventional grids time stability can only be proven for diagonal-norm SBP operators [33]. The disadvantage of diagonal-norm SBP operators is that for a $2p$ order accurate interior stencil the boundary accuracy is only p order accurate, which results in a global order of accuracy of $p + 1$ [34]. Despite this, if the discretization utilizing diagonal-norm operators is dual consistent, then the solution functionals converge at the same rate as the order of the interior operator [35, 36].

II. Notation

In accordance with [17, 20, 35], script type capital letters are used to denote continuous functions on a specific domain. For example, $\mathcal{U}(\xi) \in C^{\infty}[\xi_1, \xi_N]$ represents an infinitely differentiable function on the domain $[\xi_1, \xi_N]$. Furthermore, instances of lower case bold letters indicate the restriction of these types of functions onto a grid. For instance, $\boldsymbol{u} = [\mathcal{U}(\xi_1), \ldots, \mathcal{U}(\xi_N)]^{\mathrm{T}}$ denotes the restriction of $\mathcal{U}$ onto N nodes. In addition, small bold letters denote vectors, while sans-serif capital letters represent matrices.

A degree p SBP operator is defined as one that approximates the monomial $\boldsymbol{\xi}^k = [\xi_1^k, \ldots, \xi_N^k]^{\mathrm{T}}$ exactly, for $k = 0, 1, \ldots, p$. Here, $\boldsymbol{\xi}^k = \mathbf{0}$ if $k < 0$ by convention. As an example, if D_ξ is a one-dimensional SBP operator of degree p that approximates the derivative $\partial/\partial\xi$, then

$$\mathsf{D}_\xi \boldsymbol{\xi} = k\boldsymbol{\xi}^{k-1} \tag{1}$$

for $k = 0, 1, \ldots, p$. Therefore, we see that the degree of an SBP operator is the maximum degree of monomial for which it is exact. Also, the L_2 inner product and norm are defined for two real valued-functions, $\mathcal{U}, \mathcal{V} \in [\xi_L, \xi_R]$, as

$$(\mathcal{U}, \mathcal{V}) \equiv \int_{\xi_L}^{\xi_R} \mathcal{U}\mathcal{V}\mathrm{d}\xi, \quad \text{and} \quad ||\mathcal{U}||^2 \equiv \int_{\xi_L}^{\xi_R} \mathcal{U}^2\mathrm{d}\xi, \tag{2}$$

while the discrete inner product and norm are given by

$$(\boldsymbol{u}, \boldsymbol{v})_{\mathsf{H}} \equiv \boldsymbol{u}^{\mathrm{T}}\mathsf{H}\boldsymbol{v}, \quad \text{and} \quad ||\boldsymbol{u}||_{\mathsf{H}}^2 \equiv \boldsymbol{u}^{\mathrm{T}}\mathsf{H}\boldsymbol{u}, \tag{3}$$

respectively, where H must be symmetric and positive definite. Note also that the term "SBP operator" is used to refer to operators categorized as traditional SBP operators, as well as operators derived using the generalized framework, formally called GSBP operators. Finally, the notation related to the individual artificial dissipation operators constructed will be introduced as it appears.

III. Summation-By-Parts Operators Approximating the First Derivative

To introduce the construction of one-dimensional SBP operators, consider a scalar conservation law in one spatial dimension, given by

$$\frac{\partial \mathcal{U}}{\partial t} + \frac{\partial \mathcal{F}}{\partial x} = 0, \qquad \forall\ x \in \Omega, \qquad t \geq 0, \tag{4}$$

where $\mathcal{F}$ denotes the flux. Assuming appropriate initial and boundary conditions are applied, Eq. (4) represents a well posed problem, which means that a unique solution exists that depends continuously on the data of the problem [37]. To discretize Eq. (4), we decompose the full domain Ω into K non-overlapping elements, such that $\Omega = \bigcup_{l=1}^{K} \Omega_l$, where Ω_l denotes the l^{th} element of Ω. In principle, distinct operators could be constructed to approximate $\frac{\partial}{\partial x}$ for each individual element, Ω_l. Instead, in the present work, each element, Ω_l, is transformed from physical coordinates, x, to rectilinear computational coordinates, $\xi = \xi(x)$, using a time invariant linear mapping, and the SBP operators are constructed on the reference element spanning the computational domain $\xi \in [-1, 1]$. For clarity, suppose we are interested in discretizing the flux term in Eq. (4) using an operator constructed on the reference element defined over the computational domain, D_ξ, that approximates the first derivative. Defining $\Omega \equiv [x_{\mathrm{L}}, x_{\mathrm{R}}]$ we can relate the derivative in physical space to the derivative in reference space in one dimension as

$$\frac{\partial \mathcal{F}}{\partial x} = \frac{\mathrm{d}\xi}{\mathrm{d}x}\frac{\partial \mathcal{F}}{\partial \xi}. \tag{5}$$

In this way, a derivative operator D_x approximating $\frac{\partial}{\partial x}$ can be constructed.

For the first derivative, consider the definition of a one-dimensional SBP operator within the generalized framework, which permits operators with general nodal distributions, operators with or without one or both boundary nodes, and operators without a repeated interior point operator [20].

Definition 1. Summation-by-parts operator for the first derivative: *A matrix operator, $\mathsf{D}_\xi \in \mathbb{R}^{N\times N}$, is an SBP operator that approximates the derivative $\frac{\partial}{\partial \xi}$, on the nodal distribution $\boldsymbol{\xi} \in [\xi_{\mathrm{L}}, \xi_{\mathrm{R}}]$ having N nodes, of degree p if*

1) $\mathsf{D}_\xi \boldsymbol{\xi}^k = \mathsf{H}_\xi^{-1}\mathsf{Q}_\xi \boldsymbol{\xi}^k = k\boldsymbol{\xi}^{k-1}, \quad k = 0, 1, \ldots, p;$

2) H_ξ, *the norm matrix, is symmetric and positive definite; and*

3) $\mathsf{Q}_\xi + \mathsf{Q}_\xi^{\mathrm{T}} = \mathsf{E}_\xi$, *where* $\left(\boldsymbol{\xi}^i\right)^{\mathrm{T}} \mathsf{E}_\xi \boldsymbol{\xi}^j = \xi_{\mathrm{R}}^{i+j} - \xi_{\mathrm{L}}^{i+j}, \quad i,\ j = 0, 1, \ldots, r, r \geq p.$

To impose boundary conditions using SATs, we construct E_ξ in the following manner:

$$\mathsf{E}_\xi = \boldsymbol{t}_{\xi_{\mathrm{R}}} \boldsymbol{t}_{\xi_{\mathrm{R}}}^{\mathrm{T}} - \boldsymbol{t}_{\xi_{\mathrm{L}}} \boldsymbol{t}_{\xi_{\mathrm{L}}}^{\mathrm{T}}, \quad \text{where} \quad \boldsymbol{t}_{\xi_{\mathrm{L}}}^{\mathrm{T}} \boldsymbol{\xi}^k = \xi_{\mathrm{L}}^k, \quad \boldsymbol{t}_{\xi_{\mathrm{R}}}^{\mathrm{T}} \boldsymbol{\xi}^k = \xi_{\mathrm{R}}^k, \quad k = 0, 1, \ldots, r.$$

Here, the vectors $\boldsymbol{t}_{\xi_{\mathrm{L}}}$ and $\boldsymbol{t}_{\xi_{\mathrm{R}}}$ are known as projection operators. Furthermore, operators that have a diagonal H_ξ are know as diagonal norm operators, while operators that have a non-diagonal H_ξ are referred to as dense norm operators.

It is useful to delineate the two broad classes of SBP operators, traditional operators and element-type operators. Traditional operators utilize a repeated interior point operator to approximate a given derivative on a uniform nodal distribution that includes both boundary nodes. One-sided and biased point operators are applied near boundaries, while the same centered point operator is applied repeatedly at each node within the interior of the matrix operator, D_ξ. For traditional operators, mesh refinement is typically performed in the traditional finite-difference manner, specifically, by increasing the number of times that the repeated interior point operator is applied. Furthermore, for operators that include both boundary nodes, the projection operators accompanying Definition 1 are given by $\boldsymbol{t}_{\xi_{\mathrm{L}}} = [1, 0, \ldots, 0]^{\mathrm{T}}$ and $\boldsymbol{t}_{\xi_{\mathrm{R}}} = [0, \ldots, 0, 1]^{\mathrm{T}}$, which results in $\mathsf{E} = \mathrm{diag}(-1, 0, \ldots, 0, 1)$.

Conversely, an SBP operator without a repeated interior point operator must be implemented as an element-type operator, in which mesh refinement is performed by increasing the number of times that the element-type operator is applied, while maintaining a constant element size. For instance, consider the Legendre-Gauss quadrature nodes, which do not include boundary nodes and are found by solving $P_n = 0$, where P_n is the n^{th} Legendre polynomial given by [38]

$$P_n(\xi) = \frac{1}{2^n} \sum_{k=0}^{n} \binom{n}{k}^2 (\xi - 1)^{n-k} (\xi + 1)^k, \quad \text{for } \xi \in [-1, 1]. \tag{6}$$

As an example, a degree two element-type SBP operator constructed on the Legendre-Gauss quadrature nodes $\boldsymbol{\xi} = [-\sqrt{15}/5, 0, \sqrt{15}/5]^{\mathrm{T}}$ is given by

$$\mathsf{D}_\xi = \mathsf{H}_\xi^{-1} \mathsf{Q}_\xi = \begin{bmatrix} -\frac{1}{2}\sqrt{15} & \frac{2}{3}\sqrt{15} & -\frac{1}{6}\sqrt{15} \\ -\frac{1}{6}\sqrt{15} & 0 & \frac{1}{6}\sqrt{15} \\ \frac{1}{6}\sqrt{15} & -\frac{2}{3}\sqrt{15} & \frac{1}{2}\sqrt{15} \end{bmatrix}, \tag{7}$$

where the projection operators are given as $\boldsymbol{t}_{\xi_{\mathrm{L}}} = [(5 + \sqrt{15})/6, -2/3, (5 - \sqrt{15})/6]^{\mathrm{T}}$ and $\boldsymbol{t}_{\xi_{\mathrm{R}}} = [(5 - \sqrt{15})/6, -2/3, (5 + \sqrt{15})/6]^{\mathrm{T}}$, which are constructed using Lagrangian basis functions [20]. In contrast to traditional SBP operators, the size of the operator is fixed.

Operators with a repeating interior point operator can be applied either in the traditional manner or in an element-type manner. Operators of fixed size can only be implemented in an element-type manner.

IV. Artificial Dissipation

The use of matrix operators that utilize centered finite-difference stencils on the interior of the domain, including the majority of SBP operators, for solving nonlinear convection problems necessitates augmenting the semidiscrete scheme with a mechanism to damp spurious high-frequency modes, which provides stability and increases the overall robustness of the numerical scheme [39–41]. Although alternative methods exist for removing under-resolved high-frequency modes, for SBP operators, implementing an artificial dissipation model appears to be the most widely used means of introducing the desired level of dissipation. The use of an artificial dissipation model can also potentially improve the accuracy of a numerical simulation whose default level of dissipation is achieved through a different means, for example, element-type SBP operators coupled with upwind interface SATs.

Despite the available literature on artificial dissipation, there seems to be some confusion regarding the specific properties that a dissipation model should have. In the computational fluid dynamics community, Pulliam uses a procedure to construct boundary closures for dissipation models for use with the Euler equations that results in a negative semidefinite dissipation matrix [29]. However, while [29] demonstrates the aforementioned approach for the constant coefficient case, there is no mention of how one might translate this procedure to the variable coefficient case. In fact,

for both the fourth-difference scalar and matrix dissipation models presented in [29], that is, the models with variable coefficients, it can be shown that the dissipation matrices are not negative semidefinite in general, as [29] shows for the constant coefficient case. To appreciate this, consider the fourth-difference portion of the scalar dissipation model, S_{D}, presented in [29] that is defined to act upon the solution, u, at the j^{th} interior node by the operator

$$S_{\mathrm{D}}|_j = -\nabla b_{j+1/2} \Delta \nabla \Delta u_j, \tag{8}$$

where $\Delta u_j = u_{j+1} - u_j$ and $\nabla u_j = u_j - u_{j-1}$ are the standard forward and backward undivided difference operators, respectively, and $b_{j+1/2}$ is a variable coefficient, in this case a scalar. As an example, $b_{j+1/2}$ could be a simple average, specifically, $b_{j+1/2} = \frac{1}{2}(b_j + b_{j+1})$. Note that Eq. (8) typically includes a term that scales the dissipation with the mesh spacing; however, the scaling term has been omitted from Eq. (8) for clarity. We now prove the following theorem.

Theorem 1. *An artificial dissipation operator,* Z*, whose interior is defined by Eq. (8) is not negative semidefinite for arbitrary positive* $b_{j+1/2}$*.*

Proof. Suppose that an artificial dissipation operator, Z, is constructed whose interior entries are defined by the coefficients resulting from the application of Eq. (8) at each interior mesh node. Reorganizing Z in terms of the variable coefficient $b_{j+1/2}$ similar to the approach in [21] gives

$$\mathsf{Z} = \sum_{i=1}^{N-1} b_{j+1/2} \mathsf{M}_i, \tag{9}$$

where N denotes the number of grid nodes. We choose $N = 5$ and select a boundary closure from [29] that results in the following dissipation matrix for $b_{j+1/2} = 1$:

$$\mathsf{Z}|_{b_{j+1/2}=1} = \begin{bmatrix} -1 & 2 & -1 & 0 & 0 \\ 2 & -5 & 4 & -1 & 0 \\ -1 & 4 & -6 & 4 & -1 \\ 0 & -1 & 4 & -5 & 2 \\ 0 & 0 & -1 & 2 & -1 \end{bmatrix}. \tag{10}$$

Alternatively, for arbitrary positive $b_{j+1/2}$ Eq. (9) gives

$$\mathsf{Z} = \sum_{i=1}^{4} b_{j+1/2} \mathsf{M}_i, \tag{11}$$

where

$$\mathsf{M}_1 = \begin{bmatrix} -1 & 2 & -1 & 0 & 0 \\ 1 & -2 & 1 & 0 & 0 \\ 0 & 0 & 0 & 0 & 0 \\ 0 & 0 & 0 & 0 & 0 \\ 0 & 0 & 0 & 0 & 0 \end{bmatrix}, \quad \mathsf{M}_2 = \begin{bmatrix} 0 & 0 & 0 & 0 & 0 \\ 1 & -3 & 3 & -1 & 0 \\ -1 & 3 & -3 & 1 & 0 \\ 0 & 0 & 0 & 0 & 0 \\ 0 & 0 & 0 & 0 & 0 \end{bmatrix},$$

$$\mathsf{M}_3 = \begin{bmatrix} 0 & 0 & 0 & 0 & 0 \\ 0 & 0 & 0 & 0 & 0 \\ 0 & 1 & -3 & 3 & -1 \\ 0 & -1 & 3 & -3 & 1 \\ 0 & 0 & 0 & 0 & 0 \end{bmatrix}, \quad \mathsf{M}_4 = \begin{bmatrix} 0 & 0 & 0 & 0 & 0 \\ 0 & 0 & 0 & 0 & 0 \\ 0 & 0 & 0 & 0 & 0 \\ 0 & 0 & 1 & -2 & 1 \\ 0 & 0 & -1 & 2 & -1 \end{bmatrix}.$$

Now, a necessary and sufficient condition for Z to be negative semidefinite for arbitrary positive $b_{j+1/2}$, that is,

$$\boldsymbol{x}^{\mathrm{T}}\mathsf{Z}\boldsymbol{x} \leq 0 \quad \forall \boldsymbol{x} \in \mathbb{R}^N, \tag{12}$$

is that each of the M_i matrices must satisfy

$$\boldsymbol{x}^{\mathrm{T}}\mathsf{M}_i\boldsymbol{x} \leq 0 \quad \forall \boldsymbol{x} \in \mathbb{R}^N, \tag{13}$$

which is based on Definitions 5.3 and 5.4 of [21] and follows from the fact that the summation of two or more negative semidefinite matrices results in a negative semidefinite matrix. The condition given by Eq. (13) holds for each M_i matrix if and only if the eigenvalues of $\mathsf{M}_i + \mathsf{M}_i^{\mathrm{T}}$ are all less than or equal to zero. However, as an example, the nonzero eigenvalues of $\mathsf{M}_2 + \mathsf{M}_2^{\mathrm{T}}$ are $-6 + 2\sqrt{10}$ and $-6 - 2\sqrt{10}$, which are of opposite sign. Therefore, the fourth-difference variable coefficient artificial dissipation operator presented in [29] whose interior is defined by Eq. (8) is not negative semidefinite for arbitrary positive $b_{j+1/2}$, irrespective of the chosen boundary closure. □

Remark 1. *A fully dissipative matrix operator as defined by [29] is one that is negative semidefinite. Using this definition, we have shown that the fourth-difference variable-coefficient dissipation model introduced in [29] is not fully dissipative.*

Remark 2. *A consequence of Theorem 1 is that an SBP variable-coefficient dissipation model constructed using Eq. (8) on the interior and scaled with the appropriate norm matrix will not lead to a provably stable scheme.*

Within the SBP community, [27] constructs constant-coefficient SBP dissipation models; however, there is no discussion regarding the extension of these models to variable-coefficient scalar or matrix settings, as is done in [29]. Furthermore, it is unclear how the error introduced by the overall dissipation model vanishes in the limit of mesh refinement. In a subsequent work, Hicken introduced an SBP implementation of matrix dissipation for the Euler equations of the form [42]

$$\mathsf{Z} = -\kappa \mathsf{H}_p^{-1}\Delta_{p+1}^{\mathrm{T}}\Sigma\Delta_{p+1}, \tag{14}$$

where Δ_{p+1} is an undivided difference operator, H_p is the norm matrix associated with the overall discretization, and κ is a positive scaling factor. Furthermore, Σ is given by the block-diagonal matrix

$$\Sigma = \mathrm{diag}(|\mathsf{A}_1|, |\mathsf{A}_2|, \ldots, |\mathsf{A}_N|), \tag{15}$$

where $|\mathsf{A}_i| \equiv \mathsf{X}_i|\Lambda_i|\mathsf{X}_i^{-1}$ is the standard diagonalizable flux Jacobian matrix (as defined in [43], for example) with

$$|\Lambda_i| = \begin{bmatrix} |\lambda_{i,1}| & 0 & 0 \\ 0 & |\lambda_{i,2}| & 0 \\ 0 & 0 & |\lambda_{i,3}| \end{bmatrix}. \tag{16}$$

The form given by Eq. (14) sought to extend the artificial dissipation models in [27] to a variable-coefficient matrix setting; however, in the following theorem, we show that the matrix dissipation presented in [42] (and also used in [36]) is not negative semidefinite. This means that dissipation constructed via Eq. (14) does not lead to a provably stable semidiscrete scheme with respect to entropy or for the linearized frozen-coefficient Euler or Navier-Stokes equations via the energy method , which means that the sense in which dissipation constructed according to Eq. (14) is SBP compatible is not well defined.

Theorem 2. *The matrix $\mathsf{H}_p\mathsf{Z}$, where Z is constructed according to Eq. (14), is not negative semidefinite when Σ is defined by Eq. (15).*

Proof. Let

$$\begin{aligned} \mathsf{G} &= \mathsf{H}_p\mathsf{Z} \\ &= -\mathsf{H}_p\kappa\mathsf{H}_p^{-1}\Delta_{p+1}^{\mathrm{T}}\Sigma\Delta_{p+1} \\ &= -\kappa\Delta_{p+1}^{\mathrm{T}}\Sigma\Delta_{p+1} \end{aligned}$$

or, introducing

$$\begin{aligned}\mathsf{X} &= \operatorname{diag}(\mathsf{X}_1, \mathsf{X}_2, \ldots, \mathsf{X}_N)\\ |\Lambda| &= \operatorname{diag}(|\Lambda_1|, |\Lambda_2|, \ldots, |\Lambda_N|)\\ \mathsf{X}^{-1} &= \operatorname{diag}\left(\mathsf{X}_1^{-1}, \mathsf{X}_2^{-1}, \ldots, \mathsf{X}_N^{-1}\right)\end{aligned}$$

gives

$$\begin{aligned}\mathsf{G} &= -\kappa \Delta_{p+1}^{\mathrm{T}} \Sigma \Delta_{p+1}\\ &= -\kappa \Delta_{p+1}^{\mathrm{T}} \mathsf{X} |\Lambda| \, \mathsf{X}^{-1} \Delta_{p+1}.\end{aligned}$$

For negative semidefinite G we require

$$\boldsymbol{x}^{\mathrm{T}} \mathsf{G} \boldsymbol{x} \leq 0 \quad \forall \boldsymbol{x} \in \mathbb{R}^N. \tag{17}$$

Evaluating Eq. (17) gives

$$\begin{aligned}\boldsymbol{x}^{\mathrm{T}} \mathsf{G} \boldsymbol{x} &= -\kappa \boldsymbol{x}^{\mathrm{T}} \Delta_{p+1}^{\mathrm{T}} \mathsf{X} |\Lambda| \, \mathsf{X}^{-1} \Delta_{p+1} \boldsymbol{x}\\ &= -\kappa \underbrace{(\mathsf{X}^{\mathrm{T}} \Delta_{p+1} \boldsymbol{x})^{\mathrm{T}}}_{\text{Term \#1}} |\Lambda| \underbrace{(\mathsf{X}^{-1} \Delta_{p+1} \boldsymbol{x})}_{\text{Term \#2}}.\end{aligned}$$

Here, Term #1 and Term #2 are *not* equal, which means that we are unable to show that G is negative semidefinite. □

Remark 3. *It is possible to show that* G *is negative semidefinite if* X *is orthogonal (that is,* $\mathsf{X}^{-1} = \mathsf{X}^{\mathrm{T}}$*), which occurs when* Σ *is symmetric. This means that a scalar dissipation model, where* $\Sigma = \operatorname{diag}(\rho(\mathsf{A}_1) \times \mathsf{I}, \rho(\mathsf{A}_2) \times \mathsf{I}, \ldots, \rho(\mathsf{A}_N) \times \mathsf{I})$ *with* $\rho(\mathsf{A}_i)$ *denoting the spectral radius of* A_i *and* I *being the identity matrix, is provably stable.*

Remark 4. *Theorem 2 implies that a matrix dissipation model that is compatible with the Euler or Navier-Stokes equations in the sense of [15, 44] must be based on a symmetrized form of the governing equations, since the flux Jacobian matrices that appear in the symmetrized equations can be simultaneously diagonalized using orthogonal matrices.*

As a recent example, [32] proposed using a semidiscrete dissipation matrix of the form

$$\underbrace{-\varepsilon \left(\mathsf{H}^{-1} \mathsf{D}^{\mathrm{T}} \mathsf{H} \mathsf{A} \mathsf{D}\right)^s}_{\text{Using the notation of the present work}} \quad \text{or} \quad \underbrace{-\varepsilon \left(\underline{\underline{M}}^{-1} \, \underline{\underline{D}}^{\mathrm{T}} \, \underline{\underline{M}} \, \underline{\underline{a}} \, \underline{\underline{D}}\right)^s}_{\text{Using the notation of [32]}}, \tag{18}$$

where $s \in \mathbb{N}$ is the order, $\varepsilon \in \mathbb{R}_{>0}$ is the strength, $\underline{\underline{M}} \in \mathbb{R}^{N \times N}$ is the diagonal norm matrix, $\underline{\underline{D}} \in \mathbb{R}^{N \times N}$ is the derivative matrix, and $\underline{\underline{a}} \in \mathbb{R}^{N \times N}$ has the polynomial a projected onto the diagonal, where $a|_{\Omega_i} \geq 0$ is chosen such that $a|_{\partial\Omega_i} = 0$. Here, Ω_i denotes some domain having the surface $\partial\Omega_i$. However, the condition $a|_{\partial\Omega_i} = 0$ is not required to prove discrete conservation and stability, and is only included to interpret (18) in a well-posed continuous setting. Yet, this condition on a only seems necessary because the definition of the strength of the dissipation, ε, is ambiguous in the sense that [32] does not explicitly indicate how ε varies with the mesh spacing of the overall discretization. Understanding the allowable form of a is important as this in part dictates the general form of dissipations models that can be considered. For a consistent discretization, the original partial differential equation is recovered in the limit of mesh refinement, which implies that the contribution of the dissipation model to the discrete problem will vanish as the mesh spacing approaches zero. Therefore, aside from using arguments at the continuous level to determine the general form of the dissipation model, it is unclear what is gained by examining the dissipation model in a well-posed continuous setting. If the $a|_{\partial\Omega_i} = 0$ constraint on the polynomial a is relaxed, alternative dissipation models can be considered that have a more general structure.

V. Scalar Conservation Laws

As has been noted, the added artificial dissipation must be constructed in a careful manner such that the overall accuracy and stability properties of the underlying numerical scheme are not destroyed [27]. With these requirements in mind, consider the following SBP discretization of a partial differential equation that has been modified using an artificial dissipation model

$$\frac{\mathrm{d}\boldsymbol{u}}{\mathrm{d}t} = \mathsf{P}\boldsymbol{u} + \mathsf{A}_\mathsf{D}\boldsymbol{u}, \qquad \forall\ x \in \Omega, \qquad t \geq 0, \tag{19}$$

where $\mathsf{P}\boldsymbol{u}$ denotes a conservative and stable SBP discretization of the partial differential equation, assuming an appropriate initial condition, and A_D is the artificial dissipation operator. Note that the boundary conditions are included implicitly in the matrix operator P. Now, suppose that A_D is constructed such that

$$\frac{1}{\Delta x_{\text{avg}}^{2s-1}}\mathsf{A}_\mathsf{D}\boldsymbol{u} \approx (-1)^{s+1}\frac{\partial^s}{\partial x^s}\left(|a(x)|\frac{\partial^s \mathcal{U}}{\partial x^s}\right) \tag{20}$$

holds up to some degree of accuracy, where s is a parameter, Δx_{avg} is the average spatial mesh size, and, for now, $a(x)$ is a spatially varying scalar that has dimensions such that $\mathsf{P}\boldsymbol{u}$ and $\mathsf{A}_\mathsf{D}\boldsymbol{u}$ are dimensionally consistent. For $\Omega \equiv [x_\text{L}, x_\text{R}]$ we have

$$\Delta x_{\text{avg}} = \frac{x_\text{R} - x_\text{L}}{K(N-1)}, \tag{21}$$

where K is the number of elements used to tessellate Ω and N is the number of nodes per element.

Assuming that our underlying semidiscrete system of equations is stable, it is sufficient to examine only the stability of the dissipation model [17]. For the continuous case, substituting Eq. (20) into Eq. (19) and ignoring $\mathsf{P}\boldsymbol{u}$ gives

$$\frac{\partial \mathcal{U}}{\partial t} = (-1)^{s+1}\Delta x_{\text{avg}}^{2s-1}\frac{\partial^s}{\partial x^s}\left(|a(x)|\frac{\partial^s \mathcal{U}}{\partial x^s}\right), \qquad \forall\ x \in \Omega, \qquad t \geq 0. \tag{22}$$

To assess the stability of the continuous case, it is sufficient to investigate the stability of our partial differential equation evaluated over the l^{th} element, Ω_l, using the energy method. Specifically, we multiply Eq. (22) by the solution and integrate in space over $\Omega_l \subseteq \Omega$, which allows us to introduce the L_2 norm of the solution squared, i.e., the L_2 norm of the energy. This gives

$$\int_{\Omega_l} \mathcal{U}\frac{\partial \mathcal{U}}{\partial t}\mathrm{d}\Omega_l = \underbrace{(-1)^{s+1}\Delta x_{\text{avg}}^{2s-1}}_{\text{constant}}\int_{\Omega_l} \mathcal{U}\frac{\partial^s}{\partial x^s}\left(|a(x)|\frac{\partial^s \mathcal{U}}{\partial x^s}\right)\mathrm{d}\Omega_l. \tag{23}$$

Using Leibniz's rule combined with the definition of an L_2 norm from Eq. (2) and expanding the right-hand side using integration by parts gives

$$\frac{1}{2}\frac{\mathrm{d}||\mathcal{U}||^2}{\mathrm{d}t} = \underbrace{\Delta x_{\text{avg}}^{2s-1}\left[\sum_{i=1}^{s}(-1)^{s+i+2}\left(\frac{\partial^{i-1}\mathcal{U}}{\partial x^{i-1}}\right)\left(\frac{\partial^{s-i}}{\partial x^{s-i}}\left(|a(x)|\frac{\partial^s \mathcal{U}}{\partial x^s}\right)\right)\right]\Bigg|_{\partial\Omega_l}}_{\text{Term A}} \underbrace{-\Delta x_{\text{avg}}^{2s-1}\int_{\Omega_l}|a(x)|\left(\frac{\partial^s \mathcal{U}}{\partial x^s}\right)^2\mathrm{d}\Omega_l}_{\text{Term B}}, \tag{24}$$

where $\partial\Omega_l$ denotes the surface of Ω_l. Now, the sign of Term A in Eq. (24) is not known in general. In contrast, Term B is always negative. Therefore, Term B in Eq. (24) is a *dissipative* term because it acts to decrease the time derivative of the norm of the energy. Therefore, we seek to construct discrete artificial dissipation operators that, when evaluated using the energy method, are discretely mimetic of Term B in Eq. (24), without diminishing the accuracy of the overall discretization.

We can use the bilinear form given by Eq. (3) to directly construct a high-order approximation of Term B in Eq. (24). This gives

$$-\Delta x_{\text{avg}}^{2s-1}(\mathsf{D}^s\boldsymbol{u})^\mathsf{T}\mathsf{H}\mathsf{A}(\mathsf{D}^s\boldsymbol{u}) \approx -\Delta x_{\text{avg}}^{2s-1}\int_{x_L}^{x_R}|a(x)|\left(\frac{\partial^s \mathcal{U}}{\partial x^s}\right)^2\mathrm{d}x, \tag{25}$$

where A is the projection of $|a(x)|$ onto the diagonal, that is,

$$\mathsf{A} = \text{diag}(|a(x_1)|, |a(x_2)|, \ldots, |a(x_N)|) \tag{26}$$

and the notation D^s is equivalent to

$$\mathsf{D}^s = \underbrace{\mathsf{D}\mathsf{D}\ldots\mathsf{D}}_{s \text{ terms}}, \tag{27}$$

where D is an SBP operator approximating the first derivative. We are now ready to prove the following two theorems.

Theorem 3. *Augmenting Eq. (19) with the artificial dissipation operator given by*

$$\mathsf{A}_\mathsf{D} = -\Delta x_{\text{avg}}^{2s-1}\mathsf{H}^{-1}(\mathsf{D}^s)^\mathrm{T}\mathsf{H}\mathsf{A}(\mathsf{D}^s) \tag{28}$$

results in a stable semidiscrete scheme for diagonal and positive definite H *and diagonal and positive semidefinite* A.

Proof. Substituting Eq. (28) into Eq. (19), ignoring $\mathsf{P}\boldsymbol{u}$, and multiplying both sides by $\boldsymbol{u}^\mathrm{T}\mathsf{H}$ gives

$$\boldsymbol{u}^\mathrm{T}\mathsf{H}\frac{\mathrm{d}\boldsymbol{u}}{\mathrm{d}t} = -\boldsymbol{u}^\mathrm{T}\mathsf{H}\left(\Delta x_{\text{avg}}^{2s-1}\mathsf{H}^{-1}(\mathsf{D}^s)^\mathrm{T}\mathsf{H}\mathsf{A}(\mathsf{D}^s\boldsymbol{u})\right), \tag{29}$$

or,

$$\frac{1}{2}\frac{\mathrm{d}||\boldsymbol{u}||_\mathsf{H}^2}{\mathrm{d}t} = -\Delta x_{\text{avg}}^{2s-1}(\mathsf{D}^s\boldsymbol{u})^\mathrm{T}\mathsf{H}\mathsf{A}(\mathsf{D}^s\boldsymbol{u}), \tag{30}$$

which is stable under the above conditions. □

Theorem 4. *Augmenting Eq. (19) with the artificial dissipation operator given by*

$$\mathsf{A}_\mathsf{D} = -\Delta x_{\text{avg}}^{2s-1}\mathsf{H}^{-1}(\mathsf{D}^s)^\mathrm{T}\mathsf{H}\mathsf{A}(\mathsf{D}^s) \tag{31}$$

results in a conservative semidiscrete scheme for diagonal and positive definite H *and diagonal and positive semidefinite* A.

Proof. Substituting Eq. (31) into Eq. (19), ignoring $\mathsf{P}\boldsymbol{u}$, and multiplying both sides by $\mathbf{1}^\mathrm{T}\mathsf{H}$ gives

$$\mathbf{1}^\mathrm{T}\mathsf{H}\frac{\mathrm{d}\boldsymbol{u}}{\mathrm{d}t} = -\mathbf{1}^\mathrm{T}\mathsf{H}\left(\Delta x_{\text{avg}}^{2s-1}\mathsf{H}^{-1}(\mathsf{D}^s)^\mathrm{T}\mathsf{H}\mathsf{A}(\mathsf{D}^s\boldsymbol{u})\right), \tag{32}$$

or,

$$\mathbf{1}^\mathrm{T}\mathsf{H}\frac{\mathrm{d}\boldsymbol{u}}{\mathrm{d}t} = -\Delta x_{\text{avg}}^{2s-1}(\mathsf{D}^s\mathbf{1})^\mathrm{T}\mathsf{H}\mathsf{A}(\mathsf{D}^s\boldsymbol{u}), \tag{33}$$

but, $\mathsf{D}^s\mathbf{1} = \mathbf{0}$, so we have the final result

$$\mathbf{1}^\mathrm{T}\mathsf{H}\frac{\mathrm{d}\boldsymbol{u}}{\mathrm{d}t} = 0, \tag{34}$$

which is conservative. □

To summarize, we have shown that augmenting the right-hand side of Eq. (19) with the dissipation operator given by

$$\mathsf{A}_\mathsf{D} = -\Delta x_{\text{avg}}^{2s-1}\mathsf{H}^{-1}(\mathsf{D}^s)^\mathrm{T}\mathsf{H}\mathsf{A}(\mathsf{D}^s) \tag{35}$$

results in a conservative and stable semidiscrete scheme for scalar conservation laws.

VI. Systems of Conservation Laws

We now introduce the hyperbolic system of q equations

$$\frac{\partial\mathcal{U}}{\partial t} + \frac{\partial\mathcal{F}}{\partial x} = 0, \qquad \forall\ x \in \Omega, \qquad t \geq 0, \tag{36}$$

where $\mathcal{U} \in \mathbb{R}^{q\times 1}$ and $\mathcal{F} \in \mathbb{R}^{q\times 1}$ denotes the flux. We further assume that the system given by Eq. (36) is endowed with a convex entropy function, $\mathcal{S}_\mathrm{C}$, such that

$$\mathcal{W} \equiv \frac{\partial\mathcal{S}_\mathrm{C}}{\partial\mathcal{U}}, \tag{37}$$

where $\mathcal{W}$ are the entropy variables [45]. Therefore, for hyperbolic systems, we recast Eq. (25) in terms of the entropy variables, $\mathcal{W}$, which gives

$$-\Delta x_{\text{avg}}^{2s-1}(\mathsf{D}^s \boldsymbol{w})^{\mathrm{T}}\mathsf{H}\mathsf{A}(\mathsf{D}^s \boldsymbol{w}) \approx -\Delta x_{\text{avg}}^{2s-1}\int_{x_L}^{x_R}\left(\frac{\partial^s \mathcal{W}}{\partial x^s}\right)^{\mathrm{T}}\mathsf{A}_\alpha\left(\frac{\partial^s \mathcal{W}}{\partial x^s}\right)\mathrm{d}x, \tag{38}$$

where $\mathsf{A}_\alpha \in \mathbb{R}^{q\times q}$ is a positive semidefinite matrix, and construct the artificial dissipation using the form given by Eq. (35), where we have different options for choosing $\mathsf{A} = \text{diag}(\mathsf{A}_1, \mathsf{A}_2, \ldots, \mathsf{A}_N)$ with $\mathsf{A}_i \in \mathbb{R}^{q\times q}$ being a matrix. The constraint is that A must be positive semidefinite. For a scalar-scalar dissipation scheme, we choose

$$\mathsf{A}_i = |\lambda_{\max}|\rho\left(\frac{\partial \boldsymbol{u}_i}{\partial \boldsymbol{w}_i}\right)\times \mathsf{I}_q, \tag{39}$$

where the matrix $\frac{\partial \boldsymbol{u}_i}{\partial \boldsymbol{w}_i}$ is the symmetric positive definite entropy Jacobian at the i^{th} node whose spectral radius is denoted by $\rho\left(\frac{\partial \boldsymbol{u}_i}{\partial \boldsymbol{w}_i}\right)$, I_q is the $q\times q$ identity matrix, and $\lambda_{\max}$ is the maximum wavespeed at the i^{th} node, which is included to give A_i appropriate units. Note that we could also take the spectral radius of the product of the flux Jacobian and entropy Jacobian matrices, which may give a slightly different result. Also considered is a scalar-matrix scheme, using

$$\mathsf{A}_i = |\lambda_{\max}|\frac{\partial \boldsymbol{u}_i}{\partial \boldsymbol{w}_i}. \tag{40}$$

We do not consider a matrix-matrix scheme, because the product of the flux Jacobian matrix with the entropy Jacobian matrix is not a symmetric positive definite matrix in general. Finally, conservation for systems follows from Theorem 4, and stability follows from multiplying by the entropy variables $\boldsymbol{w}$ and integrating, analogous to Theorem 3.

VII. Artificial Dissipation for Traditional Operators

One of the drawbacks of the artificial dissipation operator given in Eq. (35) for traditional SBP operators is that applying an SBP operator approximating the first derivative, D, multiple times results in a dissipation operator whose interior stencil is wider than necessary for a given order of interior stencil. However, based on the second-derivative ideas of Del Rey Fernández *et al.* [46] and Mattsson [47] we pose an alternative artificial dissipation operator for traditional SBP operators as

$$\mathsf{A}_\mathsf{D} = -\Delta x^{2s-1}\mathsf{H}^{-1}\left[(\mathsf{D}^s)^{\mathrm{T}}\mathsf{H}\mathsf{A}(\mathsf{D}^s) - \mathsf{R}\right], \tag{41}$$

where R is constructed such that the interior stencil of the overall resultant operator is of minimum width. Furthermore, in order to prove stability for the Navier-Stokes equations, we require that R be a symmetric and negative semidefinite matrix. One such strategy is to decompose R as $-\mathsf{G}^{\mathrm{T}}\mathsf{G}$, which is negative semidefinite by construction. We also seek to construct R such that conservative nature of the underlying scheme is not destroyed. Now, in the existing literature [46, 48], suitable decompositions of R have only be proposed for the second-derivative; it has not been shown whether R decompositions of the form $-\mathsf{G}^{\mathrm{T}}\mathsf{G}$ exist for operators approximating higher-order derivatives.

Before positing a general form of R for even derivatives of arbitrary order, we will cover a brief example for clarity. Consider constructing a dissipation operator with $s = 3$ based on degree one traditional SBP operators. For this example we will examine the constant-coefficient case, i.e., we take A as the identity matrix, since the variable-coefficient case has an identical R decomposition. Furthermore, we will focus on the interior of the operator and thus we can ignore H and H^{-1} since these operators are equal to unity in the interior of the domain for a traditional SBP operator with a repeated interior point operator. Also, the dissipation operator has a leading truncation error term for each node that is proportional to a given power of the mesh spacing, Δx, which is uniform for traditional SBP operators. To keep track of the different dissipation operators, we introduce the notation $(\mathsf{A}_\mathsf{D})^{(s,b)}$, where $2s-1$ denotes the order of the interior stencil, b gives the lowest order of the boundary stencils, and $2s$ denotes the derivative that the interior stencil approximates. Therefore, for our example we have, for $s = 3$,

$$(\mathsf{A}_\mathsf{D})^{(3,:)} = -\Delta x^5\mathsf{H}^{-1}\left[(\mathsf{D}^3)^{\mathrm{T}}\mathsf{H}(\mathsf{D}^3) - \mathsf{R}\right], \tag{42}$$

where the colon indicates that we do not specify the accuracy at the boundaries of the dissipation operator. For $p = 1$, the minimum-width stencil approximating the sixth derivative is given by

$$\frac{1}{\Delta x^6}\begin{bmatrix} 1 & -6 & 15 & -20 & 15 & -6 & 1 \end{bmatrix} \propto \left.\frac{\partial^6 u}{\partial x^6}\right|_{x_j}, \tag{43}$$

where Δx is the grid spacing. Here, the stencil given by (43) is called a second-order accurate stencil because inserting Taylor expansions of the u_i about x_j in (43) results in a leading truncation error term that is proportional to Δx^2, which in this case is equal to

$$-\frac{1}{4}\Delta x^2 \left.\frac{\partial^8 u}{\partial x^8}\right|_{x_j}. \tag{44}$$

Now, consider the interior stencil for a second-order accurate operator approximating the first-derivative that uses information from three nodes, given by

$$\frac{1}{\Delta x^2}\begin{bmatrix} -\frac{1}{2} & 0 & \frac{1}{2} \end{bmatrix} \propto \left.\frac{\partial u}{\partial x}\right|_{x_j}. \tag{45}$$

Expanding the interior stencil of the term $-(\mathsf{D}^3)^{\mathrm{T}}(\mathsf{D}^3) = -(\mathsf{DDD})^{\mathrm{T}}\,\mathsf{DDD}$ from Eq. (42), where the D operator has the stencil given in (45) on the interior, results in a wide-stencil operator approximating the sixth-derivative with the following point operator at the j^{th} node:

$$\frac{1}{\Delta x^6}\begin{bmatrix} \frac{1}{64} & 0 & -\frac{3}{32} & 0 & \frac{15}{64} & 0 & -\frac{5}{16} & 0 & \frac{15}{64} & 0 & -\frac{3}{32} & 0 & \frac{1}{64} \end{bmatrix} \propto \left.\frac{\partial^6 u}{\partial x^6}\right|_{x_j}. \tag{46}$$

The objective is to construct R to reduce (46) to (43). Subtracting (46) from (43) gives the point operator for the corrective term

$$\frac{1}{\Delta x^6}\begin{bmatrix} -\frac{1}{64} & 0 & \frac{3}{32} & 1 & -\frac{399}{64} & 15 & -\frac{315}{16} & 15 & -\frac{399}{64} & 1 & \frac{3}{32} & 0 & -\frac{1}{64} \end{bmatrix}. \tag{47}$$

Further decomposing (47) as the sum of products of the form $-\mathsf{G}^{\mathsf{T}}\mathsf{G}$ is the first step in proving stability for discretizations resulting from the application of operators of the form given in Eq. (42). Therefore, inserting Taylor expansions of the u_i about x_j in (47) gives

$$-\frac{3}{4}\Delta x^2 \left.\frac{\partial^8 u}{\partial x^8}\right|_{x_j} - \frac{7}{16}\Delta x^4 \left.\frac{\partial^{10} u}{\partial x^{10}}\right|_{x_j} - \frac{2}{15}\Delta x^6 \left.\frac{\partial^{12} u}{\partial x^{12}}\right|_{x_j} + \mathcal{O}(\Delta x^8). \tag{48}$$

The first term in (48) can be approximated by applying an approximation to the fourth derivative twice; specifically, that given by the point operator

$$\frac{1}{\Delta x^4}\begin{bmatrix} \frac{1}{3} & -1 & 1 & -\frac{2}{3} & 1 & -1 & \frac{1}{3} \end{bmatrix} \propto \left.\frac{\partial^4 u}{\partial x^4}\right|_{x_j}. \tag{49}$$

Applying (49) twice gives the stencil

$$\frac{1}{\Delta x^8}\begin{bmatrix} \frac{1}{9} & -\frac{2}{3} & \frac{5}{3} & -\frac{22}{9} & 3 & -4 & \frac{14}{3} & -4 & 3 & -\frac{22}{9} & \frac{5}{3} & -\frac{2}{3} & \frac{1}{9} \end{bmatrix} \propto \left.\frac{\partial^8 u}{\partial x^8}\right|_{x_j}. \tag{50}$$

The resultant point operator approximating $-\frac{3}{4}\Delta x^2 \left.\frac{\partial^8 u}{\partial x^8}\right|_{x_j}$ is given by

$$\frac{1}{\Delta x^6}\begin{bmatrix} -\frac{1}{12} & \frac{1}{2} & -\frac{5}{4} & \frac{11}{6} & -\frac{9}{4} & 3 & -\frac{7}{2} & 3 & -\frac{9}{4} & \frac{11}{6} & -\frac{5}{4} & \frac{1}{2} & -\frac{1}{12} \end{bmatrix}. \tag{51}$$

A matrix operator with (51) in the interior can be constructed as $-\frac{3}{4}\Delta x^2(\mathsf{D}_4^{\mathsf{R}})^{\mathrm{T}}(\mathsf{D}_4^{\mathsf{R}})$. Here, the R superscript in the notation $\mathsf{D}_i^{\mathsf{R}}$ emphasizes that the operator is used in the decomposition of R and the i subscript means that the operator's interior stencil approximates the i^{th} derivative. Subtracting (51) from (47) gives the stencil

$$\frac{1}{\Delta x^6}\begin{bmatrix} \frac{13}{192} & -\frac{1}{2} & \frac{43}{32} & -\frac{5}{6} & -\frac{255}{64} & 12 & -\frac{259}{16} & 12 & -\frac{255}{64} & -\frac{5}{6} & \frac{43}{32} & -\frac{1}{2} & \frac{13}{192} \end{bmatrix}, \tag{52}$$

which approximates $\frac{5}{16}\Delta x^4 \frac{\partial^{10} u}{\partial x^{10}}\Big|_{x_j}$. The matrix operator whose interior corresponds to (52) may be constructed as $-\frac{5}{16}\Delta x^4 (\mathsf{D}_5^{\mathsf{R}})^{\mathsf{T}}(\mathsf{D}_5^{\mathsf{R}})$, where the interior of the operator $\mathsf{D}_5^{\mathsf{R}}$ is given by the stencil

$$\frac{1}{\Delta x^5}\begin{bmatrix} -\frac{1}{2} & 2 & -\frac{5}{2} & 0 & \frac{5}{2} & -2 & \frac{1}{2} \end{bmatrix} \propto \frac{\partial^5 u}{\partial x^5}\Big|_{x_j}. \tag{53}$$

Note here that the matrix operator term approximating $\frac{5}{16}\Delta x^4 \frac{\partial^{10} u}{\partial x^{10}}\Big|_{x_j}$ has a preceding negative sign because the interior stencil of $\mathsf{D}_5^{\mathsf{R}}$ given by (53) is skew symmetric. The interior stencil generated by $-\frac{5}{16}\Delta x_{\text{avg}}^4 (\mathsf{D}_5^{\mathsf{R}})^{\mathsf{T}}(\mathsf{D}_5^{\mathsf{R}})$ is given by

$$\frac{1}{\Delta x^6}\begin{bmatrix} \frac{5}{64} & -\frac{5}{8} & \frac{65}{32} & -\frac{25}{8} & \frac{75}{64} & \frac{15}{4} & -\frac{105}{16} & \frac{15}{4} & \frac{75}{64} & -\frac{25}{8} & \frac{65}{32} & -\frac{5}{8} & \frac{5}{64} \end{bmatrix}. \tag{54}$$

Since the stencil given by (53) is skew symmetric, subtracting (54) from (52) gives

$$\frac{1}{\Delta x^6}\begin{bmatrix} -\frac{1}{96} & \frac{1}{8} & -\frac{11}{16} & \frac{55}{24} & -\frac{165}{32} & \frac{33}{4} & -\frac{77}{8} & \frac{33}{4} & -\frac{165}{32} & \frac{55}{24} & -\frac{11}{16} & \frac{1}{8} & -\frac{1}{96} \end{bmatrix}, \tag{55}$$

which approximates $-\frac{1}{96}\Delta x^6 \frac{\partial^{12} u}{\partial x^{12}}\Big|_{x_j}$ and can be constructed using the matrix operator $-\frac{1}{96}\Delta x^6 (\mathsf{D}_6^{\mathsf{R}})^{\mathsf{T}}(\mathsf{D}_6^{\mathsf{R}})$, where the interior of $\mathsf{D}_6^{\mathsf{R}}$ is given by the point operator

$$\frac{1}{\Delta x^6}\begin{bmatrix} 1 & -6 & 15 & -20 & 15 & -6 & 1 \end{bmatrix} \propto \frac{\partial^6 u}{\partial x^6}\Big|_{x_j}. \tag{56}$$

Thus, the final corrective term is given as

$$\mathsf{R} = -\frac{3}{4}\Delta x^3 (\mathsf{D}_4^{\mathsf{R}})^{\mathsf{T}}(\mathsf{D}_4^{\mathsf{R}}) - \frac{5}{16}\Delta x^5 (\mathsf{D}_5^{\mathsf{R}})^{\mathsf{T}}(\mathsf{D}_5^{\mathsf{R}}) - \frac{1}{96}\Delta x^7 (\mathsf{D}_6^{\mathsf{R}})^{\mathsf{T}}(\mathsf{D}_6^{\mathsf{R}}), \tag{57}$$

where the power of Δx has been increased in each term to account for the H^{-1} term that appears at the front of Eq. (41). Note also that the decomposition of R given in Eq. (57) is a summation of terms of the form $-\mathsf{G}^{\mathsf{T}}\mathsf{G}$ which is guaranteed to be negative semi-definite as is required for proving stability. Therefore, we can pose the following general decomposition of R, which holds for even-order interior stencil operators that are arbitrarily high-order, and represents an extension of the work of Del Rey Fernández and Zingg [46] and Mattsson *et al.* [48],

$$\mathsf{R} = \sum_{i=p+s}^{2ps} \alpha_i^{(p)} \Delta x^{2(i-s)+1} (\mathsf{D}_i^{\mathsf{R}})^{\mathsf{T}} \mathsf{D}_i^{\mathsf{R}}, \tag{58}$$

where the $\alpha_i^{(p)}$ coefficients depend on both the order of the dissipation and the degree of the operator. Using this approach makes it possible to obtain minimum-width interior stencils for traditional SBP dissipation operators. There are different boundary closure options, one of which we will now discuss. The method is based on [46] and involves introducing additional degrees of freedom into the decomposition of R and then solving a system of nonlinear equations to fully specify the order of accuracy of the operator near the boundaries. With this approach, R has the general form

$$\mathsf{R} = \sum_{i=p+s}^{2ps} \alpha_i^{(p)} \Delta x^{2(i-s)+1} (\mathsf{D}_i^{\mathsf{R}})^{\mathsf{T}} \mathsf{C}_i^p \mathsf{A} \mathsf{D}_i^{\mathsf{R}}, \tag{59}$$

where C_i^p is constructed to be positive semidefinite. Therefore, the full expression for $(\mathsf{A}_{\mathsf{D}})^{(3,:)}$ may be written as

$$(\mathsf{A}_{\mathsf{D}})^{(3,:)} = -\Delta x^5 \mathsf{H}^{-1}\left[(\mathsf{D}^3)^{\mathsf{T}}\mathsf{H}\mathsf{A}(\mathsf{D}^3) + \frac{3}{4}\Delta x^3 (\mathsf{D}_4^{\mathsf{R}})^{\mathsf{T}}\mathsf{C}_4^1\mathsf{A}(\mathsf{D}_4^{\mathsf{R}}) + \frac{5}{16}\Delta x^5 (\mathsf{D}_5^{\mathsf{R}})^{\mathsf{T}}\mathsf{C}_5^1\mathsf{A}(\mathsf{D}_5^{\mathsf{R}}) + \frac{1}{96}\Delta x^7 (\mathsf{D}_6^{\mathsf{R}})^{\mathsf{T}}\mathsf{C}_6^1\mathsf{A}(\mathsf{D}_6^{\mathsf{R}})\right]. \tag{60}$$

In general, specifying the unknowns in the C_i^p and $\mathsf{D}_i^{\mathsf{R}}$ matrices in the decomposition of a given dissipation operator, for example, $(\mathsf{A}_{\mathsf{D}})^{(3,:)}$, results in the overall operator having boundary blocks in the top left and bottom right corners of the operator which contain unknowns that must be specified. There are several options available to close the boundaries of the dissipation operators, three of which we will now cover. To simplify the presentation of the operators, we examine the constant-coefficient case, recognizing that the extension to the variable-coefficient case can be performed in a straightforward manner, as exemplified by Eq. (60).

Boundary Closure Option #1: Baseline

We demonstrate the procedure for this alternative by first introducing the general structure for the artificial dissipation operator for $s = 2$, given here for the constant-coefficient case as

$$(\mathsf{A_D})^{(2,:)} = -\Delta x^3 \mathsf{H}^{-1}\left[(\mathsf{D}^2)^{\mathrm{T}}\mathsf{H}\mathsf{C}_1^1(\mathsf{D}^2) + \frac{1}{2}\Delta x^3(\mathsf{D}_3^{\mathsf{R}})^{\mathrm{T}}\mathsf{C}_3^1(\mathsf{D}_3^{\mathsf{R}}) + \frac{1}{16}\Delta x^5(\mathsf{D}_4^{\mathsf{R}})^{\mathrm{T}}\mathsf{C}_4^1(\mathsf{D}_4^{\mathsf{R}})\right], \tag{61}$$

where D is given by

$$\mathsf{D} = \frac{1}{\Delta x}\begin{bmatrix} -1 & 1 & & & & \\ -1/2 & 0 & 1/2 & & & \\ & \ddots & \ddots & \ddots & & \\ & & -1/2 & 0 & 1/2 & \\ & & & -1 & 1 \end{bmatrix}, \tag{62}$$

and the operators $\mathsf{D}_3^{\mathsf{R}}$ and $\mathsf{D}_4^{\mathsf{R}}$ are assembled as follows, where, using the baseline approach, the interior stencil is simply extended to the boundary of each operator,

$$\mathsf{D}_3^{\mathsf{R}} = \frac{1}{\Delta x^3}\begin{bmatrix} -1/2 & 1 & 0 & -1 & 1/2 & & \\ -1/2 & 1 & 0 & -1 & 1/2 & & \\ -1/2 & 1 & 0 & -1 & 1/2 & & \\ & \ddots & \ddots & \ddots & \ddots & \ddots & \\ & & -1/2 & 1 & 0 & -1 & 1/2 \\ & & -1/2 & 1 & 0 & -1 & 1/2 \\ & & -1/2 & 1 & 0 & -1 & 1/2 \end{bmatrix}, \quad \mathsf{D}_4^{\mathsf{R}} = \frac{1}{\Delta x^4}\begin{bmatrix} 1 & -4 & 6 & -4 & 1 & & \\ 1 & -4 & 6 & -4 & 1 & & \\ 1 & -4 & 6 & -4 & 1 & & \\ & \ddots & \ddots & \ddots & \ddots & \ddots & \\ & & 1 & -4 & 6 & -4 & 1 \\ & & 1 & -4 & 6 & -4 & 1 \\ & & 1 & -4 & 6 & -4 & 1 \end{bmatrix}. \tag{63}$$

For the baseline case, the C_i^1 matrices are unidiagonal with unity on the interior and s zeros near each boundary. For the present example, the C_i^1 matrices are given explicitly as

$$\begin{aligned} \mathsf{C}_1^1 &= \mathrm{diag}(0, 0, 1, 1, \ldots, 1, 1, 0, 0) \\ \mathsf{C}_3^1 &= \mathrm{diag}(0, 0, 1, 1, \ldots, 1, 1, 0, 0) \\ \mathsf{C}_4^1 &= \mathrm{diag}(0, 0, 1, 1, \ldots, 1, 1, 0, 0). \end{aligned}$$

This results in the final dissipation operator,

$$(\mathsf{A_D})^{(2,1)} = -\mathsf{H}^{-1}\begin{bmatrix} -1/4 & 1/2 & -1/4 & 0 & & & & & \\ 1/2 & -7/4 & 2 & -3/4 & & & & & \\ -1/4 & 2 & -\frac{17}{4} & 7/2 & -1 & & & & \\ 0 & -3/4 & 7/2 & -\frac{23}{4} & 4 & -1 & & & \\ & & -1 & 4 & -6 & 4 & -1 & & \\ & & & \ddots & \ddots & \ddots & \ddots & \ddots & \\ & & & & -1 & 4 & -6 & 4 & -1 \end{bmatrix} \propto \begin{matrix} -\frac{1}{4}\Delta x^2 \frac{\partial^2 u}{\partial^2 x}|_{x_j} \\ -\frac{1}{4}\Delta x^2 \frac{\partial^2 u}{\partial^2 x}|_{x_j} \\ \frac{1}{4}\Delta x^2 \frac{\partial^2 u}{\partial^2 x}|_{x_j} \\ \frac{1}{4}\Delta x^2 \frac{\partial^2 u}{\partial^2 x}|_{x_j} \\ -\Delta x^4 \frac{\partial^4 u}{\partial^4 x}|_{x_j} \\ \vdots \\ -\Delta x^4 \frac{\partial^4 u}{\partial^4 x}|_{x_j} \end{matrix}, \tag{64}$$

where the bottom right corner of the operator is a permutation of the rows and columns of the upper left portion of the operator. In general, this procedure gives operators having $2s \times 2s$ blocks in the upper left-hand and bottom right-hand corners whose stencils have a leading truncation error on the order Δx^{s-1} while the interior of the operator is of minimum width and has a leading truncation term of Δx^{2s-1}. Note that in [27] the H operator that appears at the front of the dissipation operator is an *undivided* operator and therefore the order of the interior stencil is $2s$ instead of $2s-1$; however, here we do not use an undivided H so that the dimensions of the added artificial dissipation are consistent with the rest of the discretization. Finally, Eq. (64) shows the term that each stencil approximates without accounting for the additional factor of Δx^{-1} in H^{-1}, which means that the overall operator is third-order in the interior.

Boundary Closure Option #2: Boundary-Matched

As a second alternative, we can use some of the additional degrees of freedom near the boundaries of the operator to increase the accuracy of the stencils immediately adjacent to the boundaries of the dissipation operator. Typically, the reduction in accuracy near the boundaries of a dissipation operator increases the boundary dissipation, which might cause inaccuracy in boundary layers. While this boundary approach does not increase the overall accuracy of the operator, it may be advantageous when implementing dissipation near solid wall boundaries. To describe this approach, we again consider the $s = 2$ operator defined by Eq. (61), where the constituent matrices of the overall operator are defined as

$$\mathsf{D}_3^{\mathsf{R}} = \frac{1}{\Delta x^3}\begin{bmatrix} 1 & -5 & 9 & -7 & 2 & & \\ -1/2 & 1 & 0 & -1 & 1/2 & & \\ -1/2 & 1 & 0 & -1 & 1/2 & & \\ & \ddots & \ddots & \ddots & \ddots & \ddots & \\ & & -1/2 & 1 & 0 & -1 & 1/2 \\ & & -1/2 & 1 & 0 & -1 & 1/2 \\ & & -2 & 7 & -9 & 5 & -1 \end{bmatrix}, \quad \mathsf{D}_4^{\mathsf{R}} = \frac{1}{\Delta x^4}\begin{bmatrix} 1 & -4 & 6 & -4 & 1 & & \\ 1 & -4 & 6 & -4 & 1 & & \\ 1 & -4 & 6 & -4 & 1 & & \\ & \ddots & \ddots & \ddots & \ddots & \ddots & \\ & & 1 & -4 & 6 & -4 & 1 \\ & & 1 & -4 & 6 & -4 & 1 \\ & & 1 & -4 & 6 & -4 & 1 \end{bmatrix}, \tag{65}$$

and

$$\begin{aligned} \mathsf{C}_1^1 &= \mathrm{diag}(0, 0, 0, 1, \ldots, 1, 0, 0, 0) \\ \mathsf{C}_3^1 &= \mathrm{diag}(1, 1, 1, 1, \ldots, 1, 1, 1, 1) \\ \mathsf{C}_4^1 &= \mathrm{diag}(0, 0, 1, 1, \ldots, 1, 1, 0, 0), \end{aligned}$$

which results in the overall operator

$$(\mathsf{A}_\mathsf{D})_{\mathrm{BM}}^{(2,1)} = \mathsf{H}^{-1}\begin{bmatrix} -\frac{13}{16} & \frac{13}{4} & -\frac{39}{8} & \frac{13}{4} & -\frac{13}{16} & & & & & & \\ \frac{13}{4} & -\frac{59}{4} & \frac{49}{2} & -\frac{71}{4} & \frac{19}{4} & & & & & & \\ -\frac{39}{8} & \frac{49}{2} & -\frac{89}{2} & 35 & -\frac{81}{8} & & & & & & \\ \frac{13}{4} & -\frac{71}{4} & 35 & -\frac{123}{4} & \frac{45}{4} & -1 & & & & & \\ -\frac{13}{16} & \frac{19}{4} & -\frac{81}{8} & \frac{45}{4} & -\frac{129}{16} & 4 & -1 & & & & \\ & & & -1 & 4 & -6 & 4 & -1 & & & \\ & & & & \ddots & \ddots & \ddots & \ddots & \ddots & & \\ & & & & & -1 & 4 & -6 & 4 & -1 \end{bmatrix} \propto \begin{matrix} -\frac{13}{16}\Delta x^4 \frac{\partial^4 u}{\partial^4 x}|_{x_j} \\ -\frac{1}{4}\Delta x^2 \frac{\partial^2 u}{\partial^2 x}|_{x_j} \\ -\frac{1}{4}\Delta x^2 \frac{\partial^2 u}{\partial^2 x}|_{x_j} \\ \frac{1}{4}\Delta x^2 \frac{\partial^2 u}{\partial^2 x}|_{x_j} \\ \frac{1}{4}\Delta x^2 \frac{\partial^2 u}{\partial^2 x}|_{x_j} \\ -\Delta x^4 \frac{\partial^4 u}{\partial^4 x}|_{x_j} \\ \vdots \\ -\Delta x^4 \frac{\partial^4 u}{\partial^4 x}|_{x_j} \end{matrix}, \tag{66}$$

where the stencil immediately adjacent to the boundary has the same order of leading truncation error as the interior operator. The subscript BM stands for boundary-matched and distinguishes the $(\mathsf{A}_\mathsf{D})_{\mathrm{BM}}^{(2,1)}$ operator from the $(\mathsf{A}_\mathsf{D})^{(2,1)}$

operator of the previous subsection.

Boundary Closure Option #3: Same as Mattsson, Svärd, and Nordström [27]

The third option is to construct the boundaries such that they return the same stencils in each row as those from [27] when the variable-coefficient matrix is equal to the identity matrix. For example, again for $s = 2$, using the following constituent operators

$$\mathsf{D}_3^{\mathsf{R}} = \frac{1}{\Delta x^3}\begin{bmatrix} -1/2 & 1 & 0 & -1 & 1/2 & & \\ -1 & 3 & -3 & 1 & 0 & & \\ -1/2 & 1 & 0 & -1 & 1/2 & & \\ & \ddots & \ddots & \ddots & \ddots & \ddots & \\ & & -1/2 & 1 & 0 & -1 & 1/2 \\ & & 0 & -1 & 3 & -3 & 1 \\ & & -1/2 & 1 & 0 & -1 & 1/2 \end{bmatrix}, \quad \mathsf{D}_4^{\mathsf{R}} = \frac{1}{\Delta x^4}\begin{bmatrix} 1 & -4 & 6 & -4 & 1 & & \\ 1 & -4 & 6 & -4 & 1 & & \\ 1 & -4 & 6 & -4 & 1 & & \\ & \ddots & \ddots & \ddots & \ddots & \ddots & \\ & & 1 & -4 & 6 & -4 & 1 \\ & & 1 & -4 & 6 & -4 & 1 \\ & & 1 & -4 & 6 & -4 & 1 \end{bmatrix}, \tag{67}$$

with

$$\begin{aligned} \mathsf{C}_1^1 &= \text{diag}\left(2, \frac{4}{3}, 1, 1, \ldots, 1, 1, \frac{4}{3}, 2\right) \\ \mathsf{C}_3^1 &= \text{diag}\left(0, \frac{1}{3}, 1, 1, \ldots, 1, 1, \frac{1}{3}, 0\right) \\ \mathsf{C}_4^1 &= \text{diag}(0, 0, 1, 1, \ldots, 1, 1, 0, 0), \end{aligned}$$

gives

$$(\mathsf{A}_{\mathsf{D}})^{(2,1)} = \mathsf{H}^{-1}\begin{bmatrix} -1 & 2 & -1 & & & & \\ 2 & -5 & 4 & -1 & & & \\ -1 & 4 & -6 & 4 & -1 & & \\ & \ddots & \ddots & \ddots & \ddots & \ddots & \\ & & -1 & 4 & -6 & 4 & -1 \\ & & & -1 & 4 & -5 & 2 \\ & & & & -1 & 2 & -1 \end{bmatrix} \propto \begin{matrix} -\Delta x^2 \frac{\partial^2 u}{\partial^2 x}|_{x_j} \\ \Delta x^2 \frac{\partial^2 u}{\partial^2 x}|_{x_j} \\ -\Delta x^4 \frac{\partial^4 u}{\partial^4 x}|_{x_j} \\ \vdots \\ -\Delta x^4 \frac{\partial^4 u}{\partial^4 x}|_{x_j} \\ \Delta x^2 \frac{\partial^2 u}{\partial^2 x}|_{x_j} \\ -\Delta x^2 \frac{\partial^2 u}{\partial^2 x}|_{x_j} \end{matrix}, \tag{68}$$

which has the same stencils in each row as the 4^{th}-order operator from [27].

VIII. The Quasi-One-Dimensional Euler Equations

The quasi-one-dimensional Euler equations applied to a converging-diverging nozzle on the domain $\Omega \subset \mathbb{R}^1$ are given as [49]:

$$\frac{\partial(\mathcal{S}\mathcal{Q})}{\partial t} + \frac{\partial(\mathcal{S}\mathcal{F})}{\partial x} - \mathcal{G} = 0, \quad \forall\, x \in \Omega, \quad t \geq 0, \tag{69}$$

where $\mathcal{Q} \in \mathbb{R}^{3\times 1}$, $\mathcal{F} \in \mathbb{R}^{3\times 1}$, and $\mathcal{G} \in \mathbb{R}^{3\times 1}$ denote the vector of conserved variables, the flux vector, and the source vector, respectively, defined by the relations

$$\hat{\mathcal{Q}} \equiv \mathcal{S}\mathcal{Q} = \mathcal{S}\begin{bmatrix} \rho \\ \rho u \\ e \end{bmatrix}, \quad \hat{\mathcal{F}} \equiv \mathcal{S}\mathcal{F} = \mathcal{S}\begin{bmatrix} \rho u \\ \rho u^2 + p \\ u(e+p) \end{bmatrix}, \quad \text{and} \quad \hat{\mathcal{G}} \equiv \mathcal{G} = \begin{bmatrix} 0 \\ p\frac{\mathrm{d}\mathcal{S}}{\mathrm{d}x} \\ 0 \end{bmatrix}. \tag{70}$$

Here, $e = \rho\epsilon + \frac{1}{2}\rho u^2$ and ρ, u, p, ϵ, e are density, velocity, pressure, specific internal energy, and total energy, respectively. The system is closed using a perfect gas equation, which can in turn be used to relate pressure and total energy as $e = \frac{p}{\gamma-1} + \frac{1}{2}\rho u^2$. Furthermore, $\mathcal{S} = \mathcal{S}(x)$ denotes the cross-sectional area of the converging-diverging nozzle. We consider two different functions for $\mathcal{S}(x)$, a C^∞ continuous expression, given by [50]

$$\mathcal{S}(x) \equiv -\frac{1}{250}x^3 + \frac{1}{10}x^2 - \frac{7}{10}x + \frac{5}{2} \quad \forall\ 0 \le x \le 10, \tag{71}$$

and a C^2 continuous expression, given by [49]

$$\mathcal{S}(x) \equiv \begin{cases} 1 + \frac{3}{2}\left(1 - \frac{x}{5}\right)^2 & \forall\ 0 \le x \le 5 \\ 1 + \frac{1}{2}\left(1 - \frac{x}{5}\right)^2 & \forall\ 5 < x \le 10. \end{cases} \tag{72}$$

Both subsonic and transonic problems can be defined by specifying a total inlet temperature of 300K, a total inlet pressure of 100kPa, and an outlet pressure of 92.772kPa for the subsonic problem or 86.997kPa for the C^∞ transonic problem [49]. To construct entropy-stable artificial dissipation, we introduce the entropy variables, $\mathcal{W}$, given by [23]

$$\mathcal{W} = \begin{bmatrix} \frac{\gamma-s}{\gamma-1} - \frac{1}{2}\frac{\rho}{p}u^2 \\ \frac{\rho}{p}u \\ -\frac{\rho}{p} \end{bmatrix}, \tag{73}$$

where γ denotes the ratio of specific heats and $s = \ln(p) - \gamma\ln(\rho)$ is the thermodynamic entropy. Finally, the symmetric positive definite entropy Jacobian of the conservative variables, $\mathcal{B}$, is given by [51]

$$\mathcal{B} \equiv \frac{\partial \mathcal{Q}}{\partial \mathcal{W}} = \begin{bmatrix} \rho & \rho u & e \\ \rho u & \rho u^2 + p & \rho H u \\ e & \rho H u & \rho H^2 - \frac{c^2 p}{\gamma-1} \end{bmatrix}, \tag{74}$$

where $\rho H = e + p$ defines the enthalpy, H, and the sound speed, c, is defined by $c^2 = \frac{\gamma p}{\rho}$.

Now, consider the construction of one-dimensional operators to discretize Eq. (69) using the approach outlined in Section III. Using the aforementioned approach, for the l^{th} element, $\Omega_l \subseteq \Omega$, the SBP-SAT discretization of Eq. (69) becomes

$$\frac{\mathrm{d}\hat{\boldsymbol{q}}_l}{\mathrm{d}t} + \left(\mathsf{D}_{x_l} \otimes \mathsf{I}_3\right)\hat{\boldsymbol{f}}_l - \hat{\boldsymbol{g}}_l = \mathrm{SAT}_\mathrm{L} + \mathrm{SAT}_\mathrm{R}, \tag{75}$$

where SAT_L and SAT_R are the SATs associated with the left and right interfaces of the l^{th} element, respectively, $\mathsf{I}_3 \in \mathbb{R}^3$ is an identity matrix, and $\otimes$ denotes the Kronecker product. The SAT terms in Eq. (75) are penalty terms that weakly enforce boundary conditions and inter-element coupling, where the basic premise is to simultaneously solve for the partial differential equation in combination with the boundary and interface conditions. The SATs that appear in Eq. (75) are given by

$$\mathrm{SAT}_\mathrm{L} = -\left(\mathsf{H}_{\xi_l}^{-1} \otimes \mathsf{I}_3\right) \times \left(\boldsymbol{t}_\mathrm{L} \otimes \mathsf{I}_3\right) \times \frac{1}{2}\left(\sigma\left|\tilde{\mathsf{A}}_\mathrm{L}\right| + \tilde{\mathsf{A}}_\mathrm{L}\right) \times \left(\left(\boldsymbol{t}_\mathrm{L}^\mathrm{T} \otimes \mathsf{I}_3\right)\hat{\boldsymbol{q}}_l - \left(\boldsymbol{t}_\mathrm{R}^\mathrm{T} \otimes \mathsf{I}_3\right)\hat{\boldsymbol{q}}_{l-1}\right) \tag{76}$$

$$\mathrm{SAT}_\mathrm{R} = -\left(\mathsf{H}_{\xi_l}^{-1} \otimes \mathsf{I}_3\right) \times \left(\boldsymbol{t}_\mathrm{R} \otimes \mathsf{I}_3\right) \times \frac{1}{2}\left(\sigma\left|\tilde{\mathsf{A}}_\mathrm{R}\right| - \tilde{\mathsf{A}}_\mathrm{R}\right) \times \left(\left(\boldsymbol{t}_\mathrm{R}^\mathrm{T} \otimes \mathsf{I}_3\right)\hat{\boldsymbol{q}}_l - \left(\boldsymbol{t}_\mathrm{L}^\mathrm{T} \otimes \mathsf{I}_3\right)\hat{\boldsymbol{q}}_{l+1}\right) \tag{77}$$

where $\tilde{\mathsf{A}}_{\mathrm{L}} \in \mathbb{R}^{3\times3}$ and $\tilde{\mathsf{A}}_{\mathrm{R}} \in \mathbb{R}^{3\times3}$ correspond to the flux Jacobians, $\partial\mathcal{Q}/\partial\mathcal{F}$, at averaged states at the left and right interfaces of element l, respectively. For instance, the averaged state at the left interface of the l^{th} element, $\boldsymbol{q}_{\mathrm{L,average}}$, may be evaluated by taking a simple average of the solutions of the l^{th} and $(l-1)^{\text{th}}$ elements projected onto the interface, as

$$\boldsymbol{q}_{\mathrm{L,average}} = \frac{1}{2}\left(\left(\boldsymbol{t}_{\mathrm{L}}^{\mathrm{T}} \otimes \mathsf{I}_3\right)\boldsymbol{q}_l + \left(\boldsymbol{t}_{\mathrm{R}}^{\mathrm{T}} \otimes \mathsf{I}_3\right)\boldsymbol{q}_{l-1}\right).$$

Here, $\boldsymbol{t}_{\mathrm{L}}$ and $\boldsymbol{t}_{\mathrm{R}}$ are projection operators that project, for example, the solution, $\boldsymbol{q}_l$, onto the left and right interfaces of the l^{th} element, respectively. Alternatively, a Roe-average state could be evaluated for $\boldsymbol{q}_{\mathrm{L,average}}$ [52]. Finally, the σ parameter can take the value 0, for a symmetric SAT, or 1, for an upwind SAT. We use both symmetric and upwind SATs in the present work. Note that any deviation from a symmetric SAT introduces numerical dissipation at element interfaces. As a boundary example, consider the element farthest to the left within the domain Ω. For this element, the term $\left(\boldsymbol{t}_{\mathrm{R}}^{\mathrm{T}} \otimes \mathsf{I}_3\right)\hat{\boldsymbol{q}}_{l-1}$ in Eq. (76) becomes $\hat{\boldsymbol{q}}_{\mathrm{boundary,L}} \in \mathbb{R}^{3\times1}$, where $\hat{\boldsymbol{q}}_{\mathrm{boundary,L}}$ is a vector containing boundary data for the left boundary node of Ω.

To evaluate the various artificial dissipation models, we augment Eq. (75) using the artificial dissipation model $\mathsf{A}_{\mathsf{D}}(\boldsymbol{m}_l)$, where $\boldsymbol{m}_l = \boldsymbol{q}_l$ constructs the dissipation using the conserved variables and $\boldsymbol{m}_l = \boldsymbol{w}_l$ using the entropy variables. This gives

$$\frac{\mathrm{d}\hat{\boldsymbol{q}}_l}{\mathrm{d}t} + \left(\mathsf{D}_{x_l} \otimes \mathsf{I}_3\right)\hat{\boldsymbol{f}}_l - \hat{\boldsymbol{g}}_l = \mathrm{SAT}_{\mathrm{L}} + \mathrm{SAT}_{\mathrm{R}} + \mathsf{A}_{\mathsf{D}}(\boldsymbol{m}_l)\boldsymbol{m}_l. \tag{78}$$

Note that the dissipation is applied to either $\boldsymbol{q}_l$ or $\boldsymbol{w}_l$, rather than $\hat{\boldsymbol{q}}_l$ or $\hat{\boldsymbol{w}}_l$. Furthermore, for $s = 1$ the scalar version of $\mathsf{A}_{\mathsf{D}}(\boldsymbol{q}_l)\boldsymbol{q}_l$ is algebraically equivalent to the scalar-matrix implementation of $\mathsf{A}_{\mathsf{D}}(\boldsymbol{w}_l)\boldsymbol{w}_l$; however, this is not generally the case.

IX. Numerical Results

The solution is advanced to a steady state using the implicit Euler time-marching method. The H norm of the solution error, $||\boldsymbol{e}||_{\mathsf{H}} = (\boldsymbol{e}^{\mathrm{T}}\mathsf{H}_{\mathrm{g}}\boldsymbol{e})^{1/2}$, is used to quantify the accuracy of each simulation, where $\boldsymbol{e}$ is a vector that contains the difference between the numerical solution and the exact solution at each mesh node, and H_{g} denotes the global norm matrix, which is constructed from the local element norm matrices.

At this point it is useful to introduce abbreviations for some of the different dissipation operators, which are summarized in Table 1. The simulations without any artificial dissipation model are denoted ND, while those with dissipation constructed using the baseline approach outlined in Section VII are denoted B. Element-type dissipation operators constructed on the Legendre-Gauss and Legendre-Gauss-Lobatto nodal distributions directly using Eq. (35) are also referred to as baseline operators and denoted B. The approach to assembling dissipation operators presented in [27] is modified slightly to include a variable coefficient; these we call MSN operators. The boundary-matched operators introduced in Section VII are called BM operators and SMSN refers to the operators constructed to give the same coefficients as the MSN operators for the constant-coefficient case, as outlined in Section VII. By default all dissipation operators are constructed using the conserved variables, those applied to the entropy variables are appended by the prefix "ent". Note that scalar-scalar or scalar-matrix versions of the entB operator will be denoted as they appear. Finally, P4 denotes a fourth-difference operator whose interior is defined by Eq. (8) and scaled by the proper norm matrix.

To begin, we provide numerical confirmation of Theorems 1 and 2 concerning the semidefiniteness of the fourth-difference dissipation matrices presented in [29] and [42], respectively. Figure 1 shows the eigenvalues of various dissipation models computed with a converged solution for the subsonic C^∞ nozzle problem. The models computed using the nonsymmetric matrix variable-coefficient and the biased scalar variable-coefficient have eigenvalues in the right-half plane, which confirms that these models cannot be used to prove stability for the overall discretization. In contrast, the baseline operator whose variable coefficient is the entropy-stable scalar-matrix has no eigenvalues in the right-half plane and is therefore negative semidefinite, which is a requirement for proving stability.

Figure 2 depicts the convergence results for a two-element solution to the subsonic nozzle problem with a C^∞ continuous area. A symmetric SATs is used at the element interface. Here, DOF refers to the total degrees of freedom in the spatial operator and is equal to the total number of elements multiplied by the number of nodes per element. In general, even though the exact solution is smooth, the dissipation improves the accuracy of the simulation. For the $p = 2$ case, we see that although the P4 operator is not provably stable, it still performs adequately for this specific problem. Furthermore, the performance of the SMSN operator is virtually identical to that of the MSN operator. The convergence rates that correspond to Fig. 2 are given in Table 2. In general $p + 1$ convergence is expected, which is achieved as a

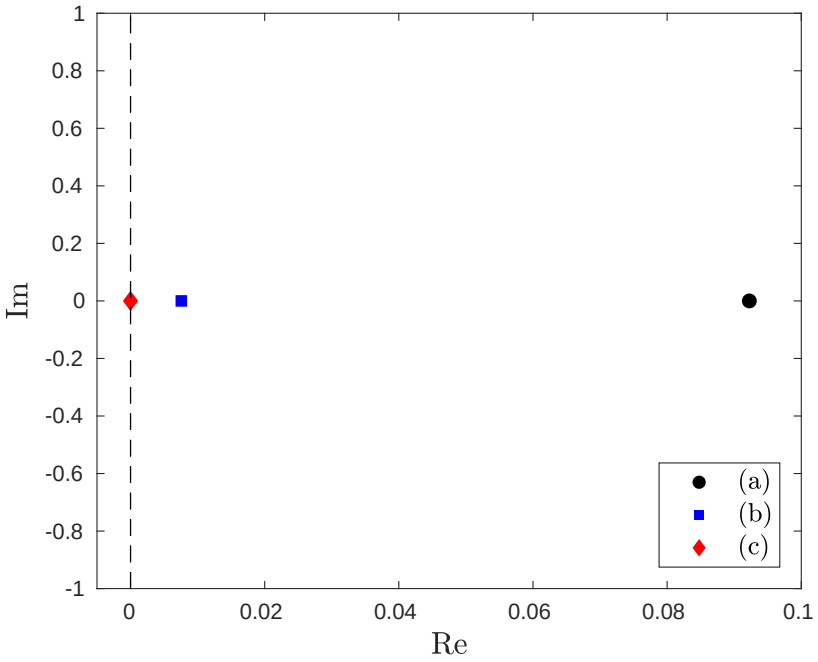

Fig. 1 Right-most eigenvalues of various dissipation models whose variable coefficient is based on a converged solution to the subsonic C^∞ nozzle problem with upwind SATs, $s = 2$, $p = 2$, and $\kappa = 1\times10^{-2}$. Three elements are used with five nodes per element. Legend key: (a) Right-most eigenvalue of $\mathsf{HZ}+(\mathsf{HZ})^{\mathrm{T}}$, where Z is a nonsymmetric matrix B operator, (b) Right-most eigenvalue of $\mathsf{HZ}+(\mathsf{HZ})^{\mathrm{T}}$, where Z is a P4 operator, (c) Right-most eigenvalue of $\mathsf{HZ}+(\mathsf{HZ})^{\mathrm{T}}$, where Z is a scalar-matrix entB operator.

minimum in all cases. Of particular note is the $p = 4$ entB operator, which achieves a convergence rate of nearly $p + 2$. To further understand the effect of the scaling factor κ, Table 3 gives the error values for different values of κ. From these results, we see that the dissipation operator can have an adverse effect if κ is too high.

Figure 3 shows the effect of increasing the number of elements while keeping the size of each element fixed. Upwind SATs are used. For the C^∞ problem, the dissipation consistently improves the accuracy of the simulation, irrespective of the number of elements. In contrast, the C^2 nozzle introduces a geometric discontinuity that causes a reduction in accuracy when an odd number of elements are used. This is not an issue when an even number of elements are used, since an interface then lies at the geometric discontinuity and only C^0 continuity is required at element interfaces.

Also considered was the difference between nonsymmetric matrix and scalar-matrix entropy-stable dissipation, these results are presented in Fig. 4 and Table 4. Two elements were used, coupled with a symmetric SAT. Overall, it appears that the scalar-matrix entropy-stable dissipation gives slightly better convergence rates and accuracy improvement over the case with no dissipation.

Figure 5 and Table 5 give the results for element-type refinement with Legendre-Gauss-Lobatto (LGL) and Legendre-Gauss (LG) operators. For these operators we exclusively use upwind SATs as element-type refinement with symmetric SATs can lead to suboptimal convergence [22]. Without dissipation, we expect $p + 1$ convergence for both the LGL and LG operators. For the LGL operators this is achieved, however for the even degree LG operators we only obtain a convergence rate of p. It is not yet understood why this reduction in accuracy is observed. When dissipation is added, the overall trend was p convergence at worst. Although a reduction in accuracy is seen for the element-type operators for smooth problems with the addition of dissipation, artificial dissipation does show a benefit for the solution of a problem with a shock. Figure 6 shows the numerical and exact solutions for the transonic problem using degree one LGL operators. It is interesting to see that using simple-average interface SATs led to lower error compared to Roe-average interface SATs, however the Roe-average SATs correctly predicted the exact location of the discontinuity. Note that the solution did not converge in the absence of artificial dissipation. Furthermore, in both cases the dissipation was applied throughout the entire domain; no local shock capturing was used.

Table 1 Abbreviations for artificial dissipation operators.

Abbreviation	*Dissipation operator*
ND	No dissipation
B	Baseline operator constructed using the new framework
entB	Entropy-stable implementation of the B operator
BM	Leading truncation error term of stencil immediately adjacent to the boundary matches that of the interior stencil
entBM	Entropy-stable implementation of the BM operator
MSN	Constructed by modifying the approach in [27] to include a variable coefficient and consistent dimensions
SMSN	Constructed using the new framework to give the same coefficients as the MSN operators for the constant-coefficient case
P4	Fourth-difference operator whose interior is defined by Eq. (8) and scaled by the appropriate norm matrix

X. Conclusion

We have described a general procedure for constructing high-order artificial dissipation operators that are compatible with the SBP approach, which means they lead to provably stable and conservative schemes. This has addressed a lack of provable stability associated with prior approaches for the case with a variable artificial dissipation coefficient. In particular, the conditions on the scalar or matrix variable artificial dissipation coefficients that lead to operators compatible with energy- or entropy-stable discretizations were outlined.

It was shown theoretically that a variable coefficient artificial dissipation operator, Z_1, whose interior is composed of the fourth-difference portion of the scalar dissipation model presented in [29] and scaled with the proper norm matrix does not lead to an artificial dissipation operator for which the eigenvalues of $\mathsf{HZ}_1 + (\mathsf{HZ}_1)^{\mathrm{T}}$ are guaranteed to lie in the left-half region of the complex plane, which means that Z_1 does not lead to provable time stability via the energy method and is therefore not compatible with the SBP approach. It was also demonstrated that a variable coefficient matrix dissipation operator, Z_2, constructed according to [42] is not one for which the eigenvalues of $\mathsf{HZ}_2 + (\mathsf{HZ}_2)^{\mathrm{T}}$ are guaranteed to lie in the left-half region of the complex plane, which means that Z_2 does not lead to provable time stability via the energy method and is therefore not compatible with the SBP approach. Finally, a variable coefficient artificial dissipation operator, Z_3, was constructed such that the eigenvalues of $\mathsf{HZ}_3 + (\mathsf{HZ}_3)^{\mathrm{T}}$ are guaranteed to lie in the left-half region of the complex plane, which means that Z_3 leads to provable time stability via the energy method and is therefore compatible with the SBP approach. The dissipation operators Z_1, Z_2, and Z_3 were used to solve a smooth problem governed by the quasi-one-dimensional Euler equations. The only variable coefficient artificial dissipation operator, Z, that has all of the eigenvalues of $\mathsf{HZ} + (\mathsf{HZ})^{\mathrm{T}}$ lie in the left-half plane is the Z_3 operator, which verifies the present framework and confirms that Z_1 and Z_2 do not lead to provably time-stable discretizations via the energy method and are therefore not compatible with the overall SBP approach.

Although the main function of artificial dissipation is to provide stabilization, it is also desirable to preserve, and potentially improve, the accuracy of the underlying discretization. The results of applying the dissipation operators to solve the quasi-one-dimensional Euler equations show that the boundary-matched and entropy-stable operators can lead to increased solution accuracy and convergence (nearing $p + 2$ for the $p = 4$ traditional operator case) for certain choices of parameters. The effectiveness of the dissipation at improving solution accuracy is diminished in the presence of a geometric discontinuity, as was seen for the C^2 nozzle, but only if the feature is not aligned with an element interface. For the element-type LG and LGL operators, a reduction in accuracy was seen for a smooth problem, but the addition of artificial dissipation was necessary to achieve convergence for a transonic problem, even when using upwind SATs. Future work will look at the application of the new dissipation operators to more complex multidimensional problems governed by the Euler and Navier-Stokes equations to see if a benefit can be achieved across a wider class of problems. Additional topics of interest are deriving entropy-stable matrix-matrix type dissipation operators that give more control over the amount of dissipation added for systems and deriving provably stable composite dissipation operators consisting of both low- and high-order interior stencils for the purpose of shock capturing.

Table 2 Convergence results corresponding to Fig. 2.

(a) $p = 1$, $s = 1$

Dissipation operator	*Slope*
ND	1.993668
MSN	2.443500
BM	2.376399
entB	2.521358
SMSN	2.443435

(b) $p = 2$, $s = 2$

Dissipation operator	*Slope*
ND	3.134411
MSN	3.210278
BM	3.217414
entBM	3.550697
SMSN	3.210265
P4	3.210268

(c) $p = 3$, $s = 3$

Dissipation operator	*Slope*
ND	4.139348
MSN	4.343410
B	4.304636
entB	4.400455

(d) $p = 4$, $s = 4$

Dissipation operator	*Slope*
ND	5.565148
MSN	5.651233
B	5.634821
entB	5.903325

Acknowledgments

The authors gratefully acknowledge the financial support provided by the Natural Sciences and Engineering Research Council of Canada and the University of Toronto.

References

[1] Wang, Z., "High-order methods for the Euler and Navier-Stokes equations on unstructured grids," *Progress in Aerospace Sciences*, Vol. 43, No. 1-3, 2007, pp. 1–41.

[2] Kreiss, H.-O., and Oliger, J., "Comparison of accurate methods for the integration of hyperbolic equations," *Tellus*, Vol. 24, No. 3, 1972, pp. 199–215.

[3] Wang, Z. J., Fidkowski, K., Abgrall, R., Bassi, F., Caraeni, D., Cary, A., Deconinck, H., Hartmann, R., Hillewaert, K., Huynh, H. T., and others, "High-order CFD methods: current status and perspective," *International Journal for Numerical Methods in Fluids*, Vol. 72, No. 8, 2013, pp. 811–845.

[4] Swartz, B., and Wendroff, B., "The relative efficiency of finite difference and finite element methods: I hyperbolic problems and splines," *SIAM Journal on Numerical Analysis*, Vol. 11, No. 5, 1974, pp. 979–993.

[5] Zingg, D. W., "Comparison of high-accuracy finite-difference methods for linear wave propagation," *SIAM Journal on Scientific Computing*, Vol. 22, No. 2, 2000, pp. 476–502.

[6] Kreiss, H.-O., and Scherer, G., "Finite Element and Finite Difference Methods for Hyperbolic Partial Differential Equations," *Mathematical Aspects of Finite Elements in Partial Differential Equations*, Academic Press, New York/London, 1974, pp. 195–212.

[7] Strand, B., "Summation by Parts for Finite Difference Approximations for d/dx," *Journal of Scientific Computing*, Vol. 20, No. 1, 1994, pp. 47–67.

[8] Hicken, J. E., and Zingg, D. W., "Parallel Newton-Krylov Solver for the Euler equations Discretized Using Simultaneous Approximation Terms," *AIAA Journal*, Vol. 46, No. 11, 2008, pp. 2773–2786.

[9] Nordström, J., Gong, J., van der Weide, E., and Svärd, M., "A stable and conservative high order multi-block method for the compressible Navier-Stokes equations," *Journal of Computational Physics*, Vol. 228, No. 24, 2009, pp. 9020–9035.

[10] Osusky, M., and Zingg, D. W., "Parallel Newton–Krylov–Schur Flow Solver for the Navier–Stokes Equations," *AIAA journal*, Vol. 51, No. 12, 2013, pp. 2833–2851.

[11] Nordström, J., and Gustafsson, R., "High order finite difference approximations of electromagnetic wave propagation close to material discontinuities," *Journal of Scientific Computing*, Vol. 18, No. 2, 2003, pp. 215–234.

[12] Calabrese, G., Lehner, L., Reula, O., Sarbach, O., and Tiglio, M., "Summation by parts and dissipation for domains with excised regions," *Classical and Quantum Gravity*, Vol. 21, No. 24, 2004, pp. 5735–5757.

[13] Funaro, D., and Gottlieb, D., "A New Method of Imposing Boundary Conditions in Pseudospectral Approximations of Hyperbolic Equations," *Mathematics of Computation*, Vol. 51, No. 184, 1988, pp. 599–613.

[14] Carpenter, M. H., Gottlieb, D., and Abarbanel, S., "Time-Stable Boundary Conditions for Finite-Difference Schemes Solving Hyperbolic Systems: Methodology and Application to High-Order Compact Schemes," *Journal of Computational Physics*, Vol. 111, 1994, pp. 220–236.

[15] Svärd, M., Carpenter, M. H., and Nordström, J., "A stable high-order finite difference scheme for the compressible Navier-Stokes equations, far-field boundary conditions," *Journal of Computational Physics*, Vol. 225, No. 1, 2007, pp. 1020–1038.

[16] Del Rey Fernández, D. C., Hicken, J. E., and Zingg, D. W., "Simultaneous Approximation Terms for Multidimensional Summation-by-parts Operators," *Journal of Scientific Computing*, Vol. 75, No. 1, 2018, pp. 83–110.

[17] Del Rey Fernández, D. C., Hicken, J. E., and Zingg, D. W., "Review of summation-by-parts operators with simultaneous approximation terms for the numerical solution of partial differential equations," *Computers & Fluids*, Vol. 95, 2014, pp. 171–196.

[18] Svärd, M., and Nordström, J., "Review of summation-by-parts schemes for initial–boundary-value problems," *Journal of Computational Physics*, Vol. 268, 2014, pp. 17–38.

[19] Nordström, J., and Svärd, M., "Well-Posed Boundary Conditions for the Navier–Stokes Equations," *SIAM Journal on Numerical Analysis*, Vol. 43, No. 3, 2005, pp. 1231–1255.

[20] Del Rey Fernández, D. C., Boom, P. D., and Zingg, D. W., "A generalized framework for nodal first derivative summation-by-parts operators," *Journal of Computational Physics*, Vol. 266, 2014, pp. 214–239.

[21] Del Rey Fernández, D. C., and Zingg, D. W., "Generalized Summation-by-Parts Operators for the Second Derivative," *SIAM Journal on Scientific Computing*, Vol. 37, No. 6, 2015, pp. A2840–A2864.

[22] Hicken, J. E., Del Rey Fernández, D. C., and Zingg, D. W., "Multidimensional Summation-by-Parts Operators: General Theory and Application to Simplex Elements," *SIAM Journal on Scientific Computing*, Vol. 38, No. 4, 2016, pp. A1935–A1958.

[23] Crean, J., Hicken, J. E., Del Rey Fernández, D. C., Zingg, D. W., and Carpenter, M. H., "Entropy-Stable Summation-By-Parts Discretization of the Euler Equations on General Curved Elements," *Journal of Computational Physics*, Vol. 356, 2018, pp. 410–438.

[24] Carpenter, M., Fisher, T., Nielsen, E., Parsani, M., Svärd, M., and Yamaleev, N., "Entropy Stable Summation-by-Parts Formulations for Compressible Computational Fluid Dynamics," *Handbook of Numerical Analysis*, Vol. 17, Elsevier, 2016, pp. 495–524.

[25] Fisher, T. C., and Carpenter, M. H., "High-order entropy stable finite difference schemes for nonlinear conservation laws: Finite domains," *Journal of Computational Physics*, Vol. 252, 2013, pp. 518–557.

[26] Mattsson, K., "Diagonal-norm upwind SBP operators," *Journal of Computational Physics*, Vol. 335, 2017, pp. 283–310.

[27] Mattsson, K., Svärd, M., and Nordström, J., "Stable and accurate artificial dissipation," *Journal of Scientific Computing*, Vol. 21, No. 1, 2004, pp. 57–79.

[28] Diener, P., Dorband, E. N., Schnetter, E., and Tiglio, M., "Optimized High-Order Derivative and Dissipation Operators Satisfying Summation by Parts, and Applications in Three-dimensional Multi-block Evolutions," *Journal of Scientific Computing*, Vol. 32, No. 1, 2007, pp. 109–145.

[29] Pulliam, T. H., "Artificial Dissipation Models for the Euler Equations," *AIAA Journal*, Vol. 24, No. 12, 1986, pp. 1931–1940.

[30] Swanson, R. C., and Turkel, E., "On central-difference and upwind schemes," *Journal of Computational Physics*, Vol. 101, No. 2, 1992, pp. 292–306.

[31] Svärd, M., and Mishra, S., "Shock Capturing Artificial Dissipation for High-Order Finite Difference Schemes," *Journal of Scientific Computing*, Vol. 39, No. 3, 2009, pp. 454–484.

[32] Ranocha, H., Glaubitz, J., Öffner, P., and Sonar, T., "Stability of artificial dissipation and modal filtering for flux reconstruction schemes using summation-by-parts operators," *Applied Numerical Mathematics*, Vol. 128, 2018, pp. 1–23.

[33] Svärd, M., "On Coordinate Transformations for Summation-By-Parts Operators," *Journal of Scientific Computing*, Vol. 20, No. 1, 2004, pp. 29–42.

[34] Gustafsson, B., "The convergence rate for difference approximations to general mixed initial boundary value problems," *SIAM Journal on Numerical Analysis*, Vol. 18, No. 2, 1981, pp. 179–190.

[35] Hicken, J. E., and Zingg, D. W., "Superconvergent Functional Estimates from Summation-By-Parts Finite-Difference Discretizations," *SIAM Journal on Scientific Computing*, Vol. 33, No. 2, 2011, pp. 893–922.

[36] Hicken, J. E., and Zingg, D. W., "Dual consistency and functional accuracy: a finite-difference perspective," *Journal of Computational Physics*, Vol. 256, 2014, pp. 161–182.

[37] Gustafsson, B., *High Order Difference Methods for Time Dependent PDE*, Springer Series in Computational Mathematics, Vol. 38, Springer Berlin Heidelberg, Berlin, Heidelberg, 2008.

[38] Koepf, W., *Hypergeometric Summation*, Universitext, Springer London, London, 2014.

[39] Von Neumann, J., and Richtmyer, R. D., "A Method for the Numerical Calculation of Hydrodynamic Shocks," *Journal of Applied Physics*, Vol. 21, No. 3, 1950, pp. 232–237.

[40] Swanson, R., and Turkel, E., "Artificial dissipation and central difference schemes for the Euler and Navier-Stokes equations," Tech. Rep. NASA CR-178296 ICASE Report No. 87-29, Institute for Computer Applications in Science and Engineering, NASA Langly Research Center, Jun. 1987.

[41] Eriksson, L.-E., "Boundary Conditions for Artifcial Dissipation Operators," Tech. Rep. FFA TN 1984-53, The Aeronautical Research Institute of Sweden, Aerodynamics Department, 1984.

[42] Hicken, J. E., "Output error estimation for summation-by-parts finite-difference schemes," *Journal of Computational Physics*, Vol. 231, No. 9, 2012, pp. 3828–3848.

[43] Pulliam, T. H., and Chaussee, D. S., "A diagonal form of an implicit approximate-factorization algorithm," *Journal of Computational Physics*, Vol. 39, No. 2, 1981, pp. 347–363.

[44] Svärd, M., and Nordström, J., "A stable high-order finite difference scheme for the compressible Navier-Stokes equations, no-slip wall boundary conditions," *Journal of Computational Physics*, Vol. 227, No. 10, 2008, pp. 4805–4824.

[45] Tadmor, E., "Entropy stability theory for difference approximations of nonlinear conservation laws and related time-dependent problems," *Acta Numerica*, Vol. 12, 2003, pp. 451–512.

[46] Del Rey Fernández, D. C., and Zingg, D. W., "Generalized Summation-By-Parts Operators for the Second Derivative," *SIAM Journal on Scientific Computing*, Vol. 37, No. 6, 2015, pp. A2840–A2864.

[47] Mattsson, K., "Summation by Parts Operators for Finite Difference Approximations of Second-Derivatives with Variable Coefficients," *Journal of Scientific Computing*, Vol. 51, No. 3, 2012, pp. 650–682.

[48] Mattsson, K., Svärd, M., and Shoeybi, M., "Stable and accurate schemes for the compressible Navier–Stokes equations," *Journal of Computational Physics*, Vol. 227, No. 4, 2008, pp. 2293–2316.

[49] Pulliam, T. H., and Zingg, D. W., *Fundamental Algorithms in Computational Fluid Dynamics*, Scientific Computation, Springer International Publishing, 2014.

[50] Huan, X., Hicken, J., and Zingg, D., "Interface and boundary schemes for high-order methods," *19th AIAA Computational Fluid Dynamics Conference*, 2009, pp. 1–10.

[51] Gassner, G. J., Winters, A. R., and Kopriva, D. A., "Split form nodal discontinuous Galerkin schemes with summation-by-parts property for the compressible Euler equations," *Journal of Computational Physics*, Vol. 327, 2016, pp. 39–66.

[52] Roe, P. L., "Approximate Riemann solvers, parameter vectors, and difference schemes," *Journal of Computational Physics*, Vol. 43, No. 2, 1981, pp. 357–372.

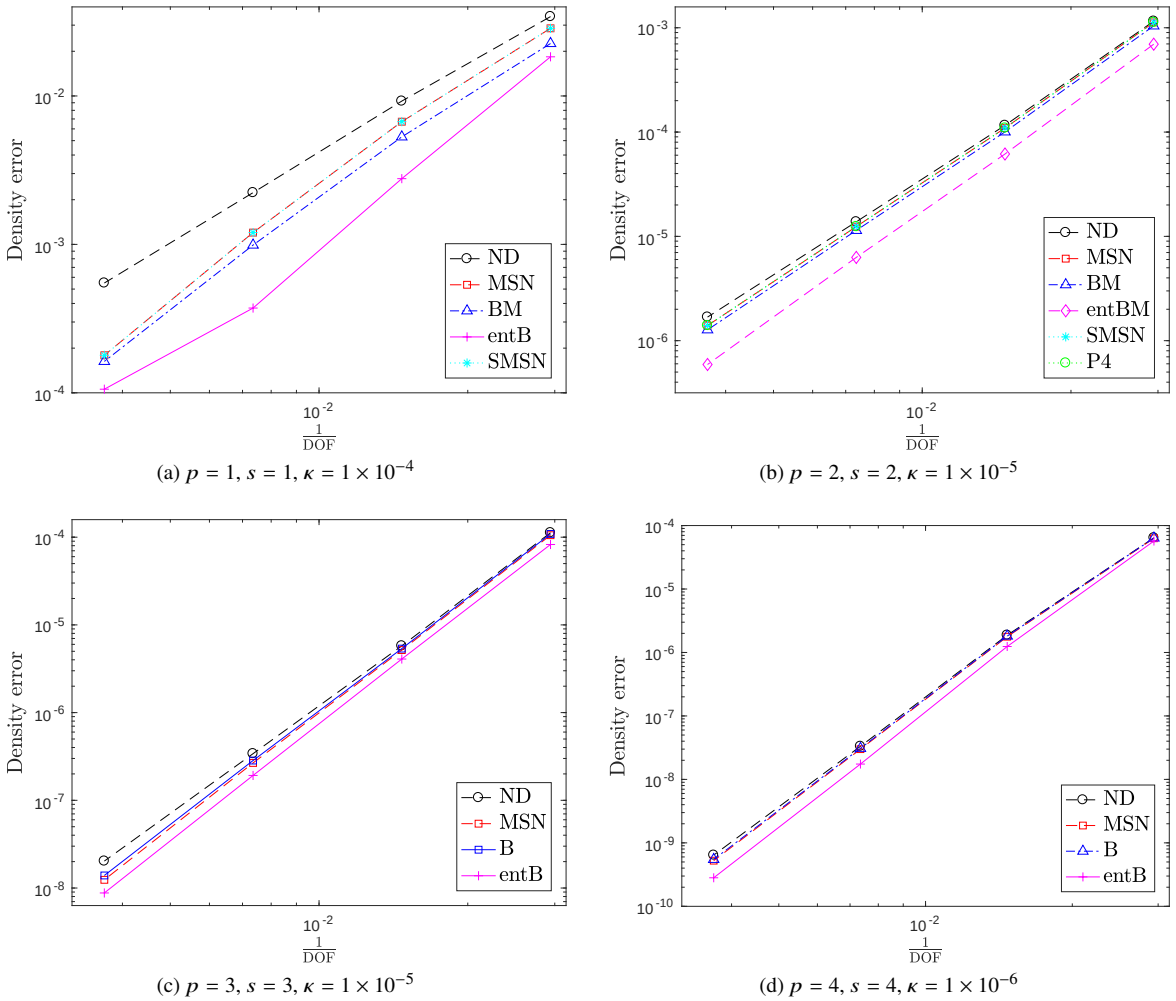

(a) $p = 1$, $s = 1$, $\kappa = 1 \times 10^{-4}$

(b) $p = 2$, $s = 2$, $\kappa = 1 \times 10^{-5}$

(c) $p = 3$, $s = 3$, $\kappa = 1 \times 10^{-5}$

(d) $p = 4$, $s = 4$, $\kappa = 1 \times 10^{-6}$

Fig. 2 Convergence of the H norm of the density error using a variety of scalar artificial dissipation operators with traditional refinement for the subsonic C^∞-nozzle problem. Two elements are used, coupled with a symmetric SAT ($\sigma = 0$). The entB operators use a scalar-scalar variable coefficient. Legend key: ND = no dissipation, B = baseline, entB = entropy-stable baseline, BM = boundary-matched, MSN = modified approach from [27], SMSN = same as MSN for constant-coefficient case, P4 = fourth-difference interior defined by Eq. (8).

Table 3 Density error for different values κ for scalar artificial dissipation models. Upwind SATs are used ($\sigma = 1$) with 20 nodes per element. $p = 2$, $s = 2$.

κ	*Number of elements*	*Dissipation operator*	*Density error* $\left[\mathrm{kg\,m^{-3}}\right]$
1×10^{0}	2	ND	$4.978\,560 \times 10^{-4}$
1×10^{0}	2	SMSN	$5.368\,979 \times 10^{-3}$
1×10^{0}	2	BM	$3.460\,109 \times 10^{-3}$
1×10^{0}	4	ND	$5.247\,656 \times 10^{-5}$
1×10^{0}	4	SMSN	$1.027\,667 \times 10^{-3}$
1×10^{0}	4	BM	$7.857\,045 \times 10^{-4}$
1×10^{0}	8	ND	$6.369\,965 \times 10^{-6}$
1×10^{0}	8	SMSN	$2.232\,947 \times 10^{-4}$
1×10^{0}	8	BM	$1.817\,209 \times 10^{-4}$
1×10^{-1}	2	ND	$4.978\,560 \times 10^{-4}$
1×10^{-1}	2	SMSN	$8.147\,959 \times 10^{-4}$
1×10^{-1}	2	BM	$5.410\,338 \times 10^{-4}$
1×10^{-1}	4	ND	$5.247\,656 \times 10^{-5}$
1×10^{-1}	4	SMSN	$1.502\,759 \times 10^{-4}$
1×10^{-1}	4	BM	$1.053\,608 \times 10^{-4}$
1×10^{-1}	8	ND	$6.369\,965 \times 10^{-6}$
1×10^{-1}	8	SMSN	$3.281\,348 \times 10^{-5}$
1×10^{-1}	8	BM	$2.273\,909 \times 10^{-5}$
1×10^{-2}	2	ND	$4.978\,560 \times 10^{-4}$
1×10^{-2}	2	SMSN	$2.200\,478 \times 10^{-4}$
1×10^{-2}	2	BM	$2.153\,270 \times 10^{-4}$
1×10^{-2}	4	ND	$5.247\,656 \times 10^{-5}$
1×10^{-2}	4	SMSN	$2.944\,840 \times 10^{-5}$
1×10^{-2}	4	BM	$2.952\,823 \times 10^{-5}$
1×10^{-2}	8	ND	$6.369\,965 \times 10^{-6}$
1×10^{-2}	8	SMSN	$5.047\,127 \times 10^{-6}$
1×10^{-2}	8	BM	$4.387\,419 \times 10^{-6}$
1×10^{-3}	2	ND	$4.978\,560 \times 10^{-4}$
1×10^{-3}	2	SMSN	$4.177\,050 \times 10^{-4}$
1×10^{-3}	2	BM	$2.957\,571 \times 10^{-4}$
1×10^{-3}	4	ND	$5.247\,656 \times 10^{-5}$
1×10^{-3}	4	SMSN	$4.268\,613 \times 10^{-5}$
1×10^{-3}	4	BM	$3.184\,621 \times 10^{-5}$
1×10^{-3}	8	ND	$6.369\,965 \times 10^{-6}$
1×10^{-3}	8	SMSN	$4.784\,153 \times 10^{-6}$
1×10^{-3}	8	BM	$3.910\,360 \times 10^{-6}$

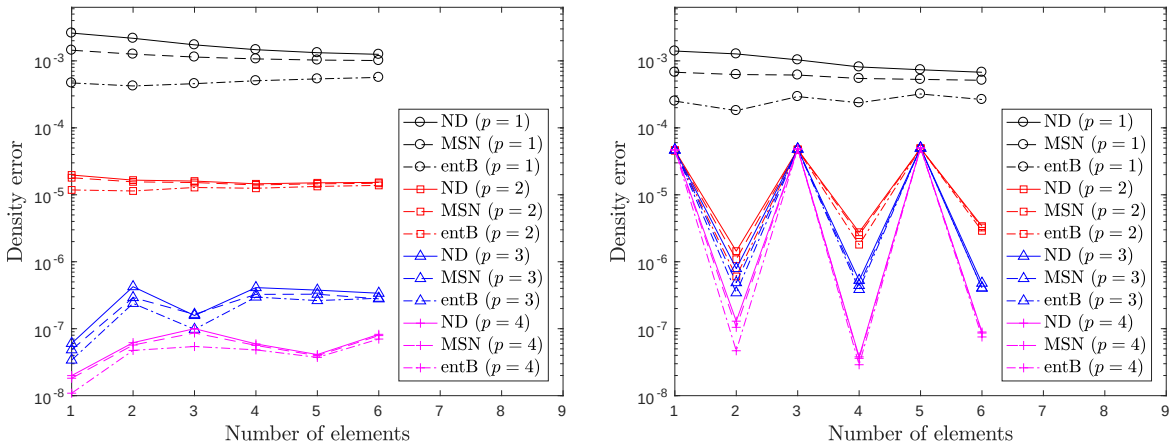

(a) C^∞ continuous nozzle

(b) C^2 continuous nozzle

Fig. 3 Density error as a function of number of elements for a constant number of degrees of freedom. Upwind SATs are used. For all operators, $s = p$. Legend key: ND = no dissipation, entB = entropy-stable baseline, BM = boundary-matched, MSN = modified approach from [27].

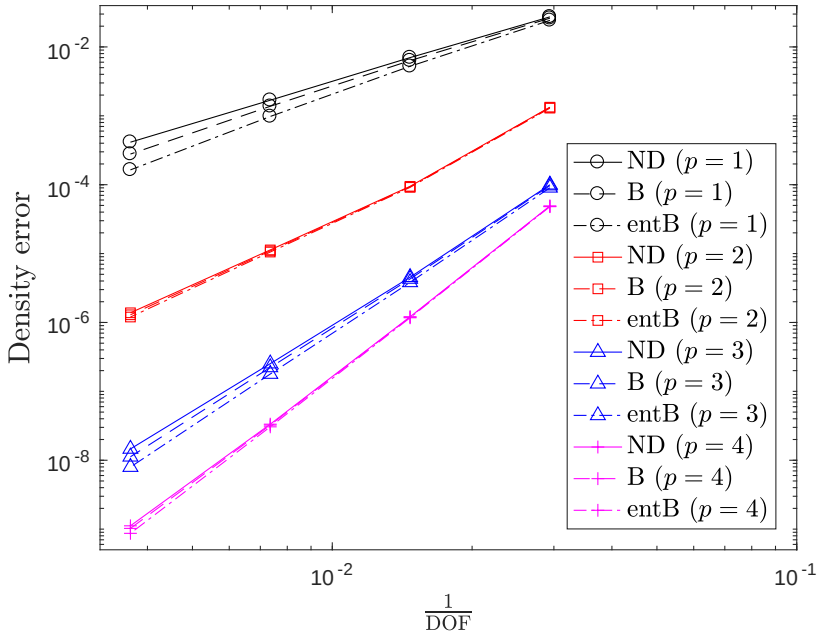

Fig. 4 Convergence of the H norm of the density error using a nonsymmetric matrix B operator and an entropy-stable symmetric scalar-matrix entB operator with traditional refinement for the subsonic nozzle problem. Two elements are used, coupled with a symmetric SAT. For all operators, $s = p$. Legend key: ND = no dissipation, B = baseline, entB = entropy-stable baseline.

Table 4 Convergence results corresponding to Fig. 4.

Dissipation operator	*Degree*	*Slope*
ND	1	2.018651
B	1	2.185594
entB	1	2.404795
ND	2	3.281156
B	2	3.308163
entB	2	3.333904
ND	3	4.238811
B	3	4.349376
entB	3	4.482478
ND	4	5.144717
B	4	5.181173
entB	4	5.252103

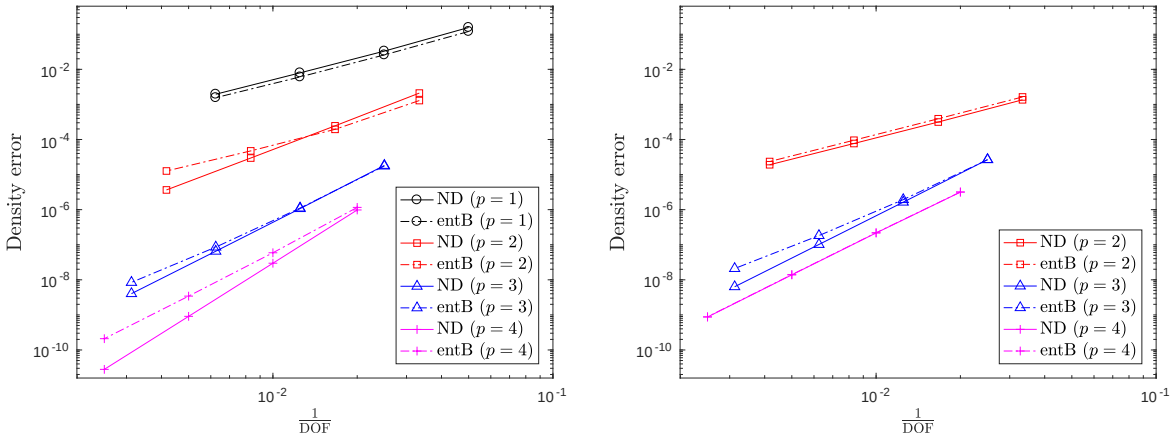

(a) Dissipation with Legendre-Gauss-Lobatto operators

(b) Dissipation with Legendre-Gauss operators

Fig. 5 Convergence of the H norm of the density error using scalar and scalar-scalar entropy-stable dissipation for the subsonic C^∞ nozzle problem. Upwind SATs are used ($\sigma = 1$). For all operators, $s = p$. Legend key: ND = no dissipation, entB = entropy-stable baseline.

Table 5 Convergence results corresponding to Fig. 5.

(a) Legendre-Gauss-Lobatto

Dissipation operator	*Degree*	*Slope*
ND	1	2.101912
entB	1	2.089688
ND	2	3.056819
entB	2	2.205590
ND	3	4.045845
entB	3	3.675173
ND	4	5.031773
entB	4	4.139951

(b) Legendre-Gauss

Dissipation operator	*Degree*	*Slope*
ND	2	2.048818
entB	2	2.038130
ND	3	4.011971
entB	3	3.432788
ND	4	3.945651
entB	4	3.942748

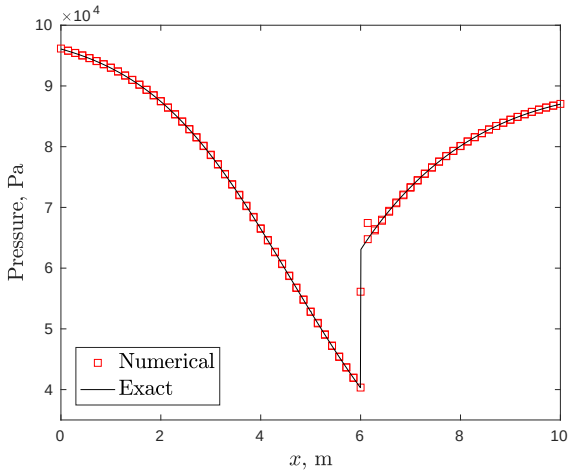

(a) Roe-average SATs, Density error = $6.317\,680 \times 10^{-2}$ kg m^{-3}

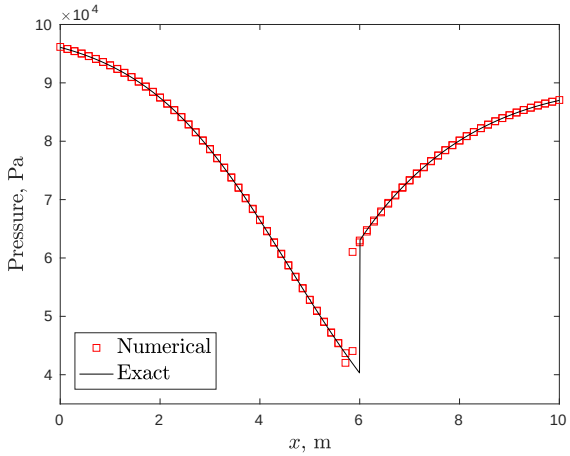

(b) Simple-average SATs, Density error = $5.136\,893 \times 10^{-2}$ kg m^{-3}

Fig. 6 Numerical and exact solutions for the transonic C^∞ nozzle problem using two different upwind interface SATs. Legendre-Gauss-Lobatto operators are used with 70 elements and scalar-matrix entropy-stable baseline dissipation. $p = 1$, $s = 1$, $\kappa = 2 \times 10^{-3}$.